Master Thesis

Development of the Java-based Simulator for IceCube

02UM1102

Rie Ishibashi

A thesis submitted in partial fulfillment
of the requirements of the degree of Master of Science

at

Graduate School of Science and Technology

Chiba University

Abstract

The IceCube is an underground neutrino observatory now under construction at the south pole. The advantages of the observation of the universe by neutrinos are that they can arrive on the earth directly from the sources without deflection by magnetic fields, and that they penetrate stars, gas and galaxies because they rarely interact with matters and radiations during their journey. Therefore the neutrinos can propagate without losing the information of their sources.

In order to determine the energy and direction of extremely high energy (EHE) neutrinos with energies up to $\sim 10^{20}$eV, the energy deposit as Cherenkov light emission from electromagnetic and hadronic cascades in ice must be measured. However, the energy deposit behavior has the stochastic nature in ultra high energy range which can not be properly calculated by analytic calculations, because the interactions and decay give rise to not a continuous energy loss but a stochastic loss.

Therefore we developed the Monte-Carlo/Numerical simulator named **JULIeT** – **Java-based Ultra high energy Leptons IntEgral Transportor**. It provides two features to simulate the EHE particle propagation. The numerical calculations are used to study the propagation of neutrinos and charged leptons in Earth over long courses. Secondary produced EHE cosmic neutrinos and charged leptons are also followed by our numerical calculation. The Monte-Carlo simulations are used to obtain the distributions of energy deposit in the deep-ice detector. By convoluting the propagation in the earth and the energy deposit in the detector, we can evaluate the IceCube sensitivity on EHE neutrino detection.

The 90% C.L. IceCube sensitivity for primary EHE neutrino flux has been found to be placed at $E^2 dF/dE \simeq 2.1 \times 10^{-8}$ [GeV cm^{-2} sec $^{-1}$ sr $^{-1}$] for the primary ν_μ and ν_τ with 10^9 GeV in absence of signals with energy deposit of 10 PeV or greater.

Acknowledgments

I would like to express sincere gratitude to my supervisors, Prof. S. Yoshida and Prof. H. Kawai, for their support and advice in this work.

I would like to thank all of the members of Chiba IceCube group, Dr. K.Hoshina, H. Miyamoto, K. Fujimoto, T. Noda for their suggestions and help.

I would also like to thank H. Nakayama, T. Ooba, Y. Shiino, Y. Unno, N. Orita, T. Tsuda, H. Uchiyama, M. Konishi, T. Nunomura, Y. Ono, M. Tabata, N. Inadama, S. Saitoh. They always supported and helped me, and I enjoyed my study and day life with them.

I am very grateful to my parents for their support and encouragement.

Contents

1 Introduction **1**
- 1.1 Introduction of EHE Neutrino Astrophysics . . . 1
- 1.2 Detection Method : Overview . . . 1
- 1.3 IceCube : The Underground Neutrino Observatory at the South Pole . . . 2

2 Propagation of Neutrinos and Charged Leptons **5**
- 2.1 Interactions of Neutrinos and Charged Leptons . . . 5
  - 2.1.1 Neutrino Interaction . . . 5
  - 2.1.2 Charged Lepton Interaction . . . 6
- 2.2 Decays of Charged Leptons . . . 11
- 2.3 Issues and Motivation . . . 12

3 Development of Java-based MonteCarlo/Numerical Simulator **14**
- 3.1 Design Policy . . . 14
- 3.2 Structure of JULIeT . . . 14
  - 3.2.1 Points Package . . . 16
  - 3.2.2 Particles Package . . . 16
  - 3.2.3 Interactions Package . . . 16
  - 3.2.4 Decay Package . . . 16
  - 3.2.5 Propagation Package . . . 19
  - 3.2.6 Event Package . . . 20
- 3.3 Simulated Results . . . 23

4 IceCube Sensitivity for EHE Neutrinos **30**
- 4.1 Flux of Neutrinos and Charged Leptons at IceCube Depth . . . 30
  - 4.1.1 GZK Neutrinos . . . 30
  - 4.1.2 Z-burst . . . 31
  - 4.1.3 Top Down Scenario . . . 31
- 4.2 Background . . . 31
- 4.3 Flux at the IceCube Depth . . . 32
- 4.4 Evaluation of IceCube Sensitivity . . . 34

5 Summary and Outlook **38**
- 5.1 Summary . . . 38
- 5.2 Future Work . . . 38

List of Figures

1.1 IceCube:Underground Neutrino Observatory . . . 3
1.2 Schematic View of Digital Optical Module . . . 3
1.3 Top View of IceCube Observatory . . . 4
1.4 DOM Arrangement . . . 4

2.1 Cross Sections . . . 6

3.1 Package Structure of the JULIeT . . . 15
3.2 Class Structure of the JULIeT –propagation . . . 17
3.3 Class Structure of the JULIeT –event . . . 18
3.4 Definition of geometric parameters . . . 19
3.5 Distribution of Energy Deposit in Ice for Muon . . . 25
3.6 Distribution of Energy Deposit in Ice for Muon . . . 25
3.7 Distribution of Energy Deposit in Ice for Tau . . . 26
3.8 Distribution of Energy Deposit in Ice for Tau . . . 26
3.9 Dependence of Energy Deposit on the Primary Energy for Muon . . . 27
3.10 Dependence of Energy Deposit on the Primary Energy for Tau . . . 27
3.11 Dependence of the Range on the Primary Energy for μ and τ . . . 28
3.12 Distribution of Energy Deposit of Each Interaction/Decay in Ice for ν_μ . . . 29

4.1 Angular Distribution of Charged Lepton flux . . . 33
4.2 Angular Distribution of Energy Deposit in the Detector . . . 33
4.3 IceCube Sensitivities on EHE Neutrino Fluxes for ν_μ and for ν_τ . . . 35
4.4 IceCube Sensitivities on EHE Neutrino Fluxes . . . 36

List of Tables

2.1 Parameters in ALLM97 parametrization 11

3.1 Channels of Infinitesimal Propagation 15
3.2 Channels of Interaction/Decay for Monte-Carlo Simulation 21

4.1 EHE Neutrino Models 31
4.2 90% C.L. Upper Limit for EHE Neutrino Fluxes 37

Chapter 1

Introduction

1.1 Introduction of EHE Neutrino Astrophysics

The observation of high energy neutrinos provides a new window to search for high energy phenomena in universe. Neutrinos can arrive on the earth directly from the sources, because they have no charge and they are not deflected by magnetic fields. Additionally, neutrinos interact only weakly, so they rarely interact in their journey.

The extremely high energy (EHE) neutrinos with energies up to 10^{20} eV may be produced by mechanisms such as the Greisen-Zatsepin-Kuzmin (GZK) mechanism [1]. The GZK neutrinos via decays of charged pions produced by photo-pion production of EHE cosmic rays (EHECRs) colliding cosmic microwave background (CMB) photons. In this production mechanism no ν_τs are generated because the pion-muon decay chain,

$$\begin{aligned} p\gamma &\rightarrow \pi^{\pm} + anything \\ &\rightarrow \mu^{\pm} + \nu_\mu(\bar{\nu}_\mu) \\ &\rightarrow e^{\pm} + \nu_e(\bar{\nu}_e) + \bar{\nu}_\mu(\nu_\mu), \end{aligned}$$

does not have any channel to produce ν_τ. By the interaction of EHECRs and CMBs, EHECRs lose their own energy during their propagation. Therefore the spectrum of EHECRs should have a *cut-off* feature at around 5×10^{19} eV. This "GZK cut-off" has not clearly seen in the observed data. Whether the GZK mechanism, the most solid model of EHE neutrino radiation, takes place in the present universe still remains a mystery.

There are a lot of other hypotheses to predict EHE neutrinos. The observation of EHE neutrinos and the search of their sources lead to new understanding of high energy universe.

1.2 Detection Method : Overview

Because the cross sections of the neutrino interactions in this energy range are enhanced, they interact with the nuclei of medium in the earth and produce neutrinos or charged leptons via neutral current interaction (NC) or charged current interaction (CC);

$$\begin{aligned} \nu_l(\bar{\nu}_l) + N &\rightarrow \nu_l(\bar{\nu}_l) + X \quad (NC), \\ \nu_l(\bar{\nu}_l) + N &\rightarrow l^{\mp} + X \quad\quad (CC), \end{aligned}$$

where N is a nucleon of the medium, l is charged lepton (e, μ, τ), X is produced hadrons.

Hadrons produced via NC or CC induce a hadronic cascade, and an electron produced via CC initiates an electromagnetic cascade. Therefore EHE particles arriving at an underground detector are not just primary neutrinos but secondary produced ν's, μ's, and τ's.

When a charged particle propagates in transparent medium with the speed faster than that of light in the medium, the Cherenkov light is emitted. The number of radiated photons is proportional to path length, and the emission angle depends on the refractive index of the medium. By seeing emitted Cherenkov light and its angle, we can detect the charged particle and reconstruct the event track.

When an EHE particle propagate in a detector, the induced cascades contain many charged particles which emit a bulk of the Cherenkov photons. Amount of such Cherenkov light packets is an estimator of energy deposit of an EHE particle.

1.3 IceCube : The Underground Neutrino Observatory at the South Pole

The IceCube is the underground neutrino observatory now under construction at the south pole. It is the *telescope* to explore the high energy universe with cosmic neutrinos emitted from energetic distant sources. Since only neutrinos can penetrate underground, the earth is an effective shield to eliminate high energy primary particles except neutrinos (See Figure 1.1). The main backgrounds are atmospheric muons and neutrinos which will be described in details in section 4.2.

The flux of EHE neutrinos that arrive at the earth is very small. Therefore we need a detector with large target volume. The detector of the IceCube is made of polar *ice* with the volume of 1km^3. It is made of natural glacial ice with the depth from $1400m$ to $2400m$ under the ice surface. The glacial polar ice is suitable for the neutrino telescope like the IceCube [2] as demonstrated by the AMANDA experiment.

Neutrinos produced via NC, or charged leptons produced via CC can produce electromagnetic and/or hadronic cascades by interactions. When a cascade is produced in the detector, the cascade particles induce the Cherenkov light. The IceCube observes the neutrinos by detecting the Cherenkov light from these cascades using many photomultiplier tubes (PMTs) instrumented in ice.

The IceCube detector will instrument the 4800 PMTs which have 10 inch diameter. These PMTs will be buried in vertical holes of ice drilled by hot water, so they have to endure very high pressure and low temperature. Therefore each PMT is put in the pressure glass sphere comprise a digital optical module (DOM). The IceCube DOMs contain a signal processing electronics board, a LED flasher for calibration, and a high voltage supplier. Figure 1.2 shows the schematic view of the DOM. The PMT in the glass sphere is supported by gel as a shock absorber.

These DOMs will be arrayed on 80 strings, which contains 60 DOMs spaced by $17m$. Each string are spaced $125m \sim$ (Figure 1.3) and instrumented in the vertical holes of ice such as Figure 1.4.

We can obtain the profile of the EHE ν-induced cascades by detecting the Cherenkov light hit at many DOMs arranged three dimensionally.

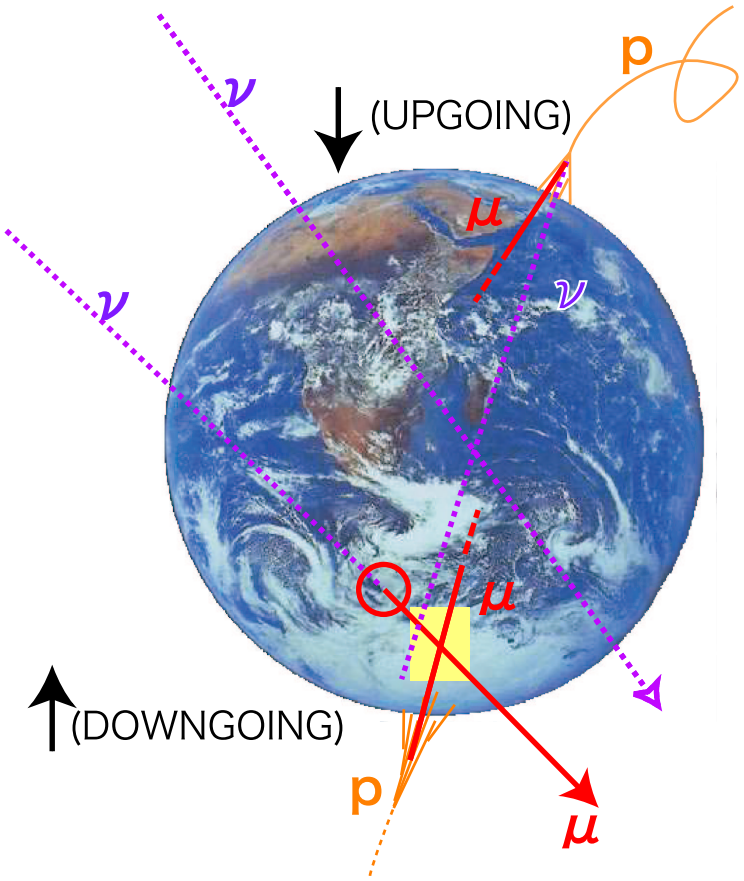

Figure 1.1: IceCube is the underground neutrino observatory. It uses the earth as a shield to cut the backgrounds.

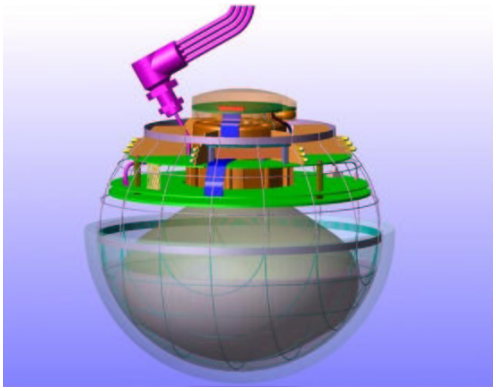

Figure 1.2: Schematic view of the Digital Optical Module (DOM) for the IceCube. It contains a PMT, electronics board, LED flasher for calibration and a high voltage supplier. They are protected by pressure glass sphere.

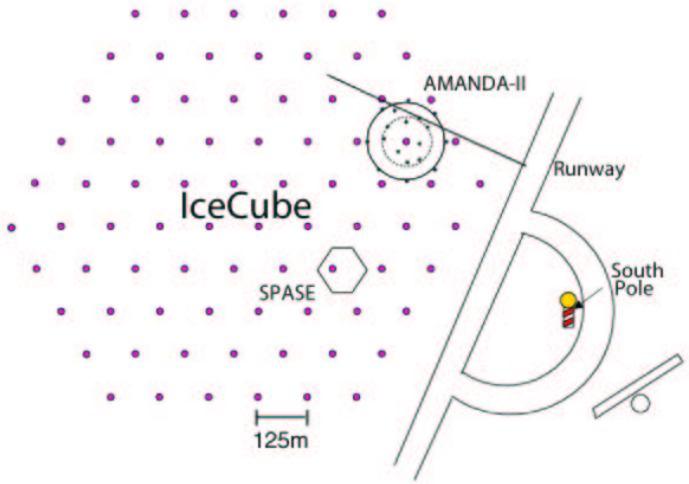

Figure 1.3: Top view of the IceCube observatory. The 60 DOMs will be arrayed on 80 strings which are spaced by $125m \sim$. Each string is instrumented in the vertical holes of ice.

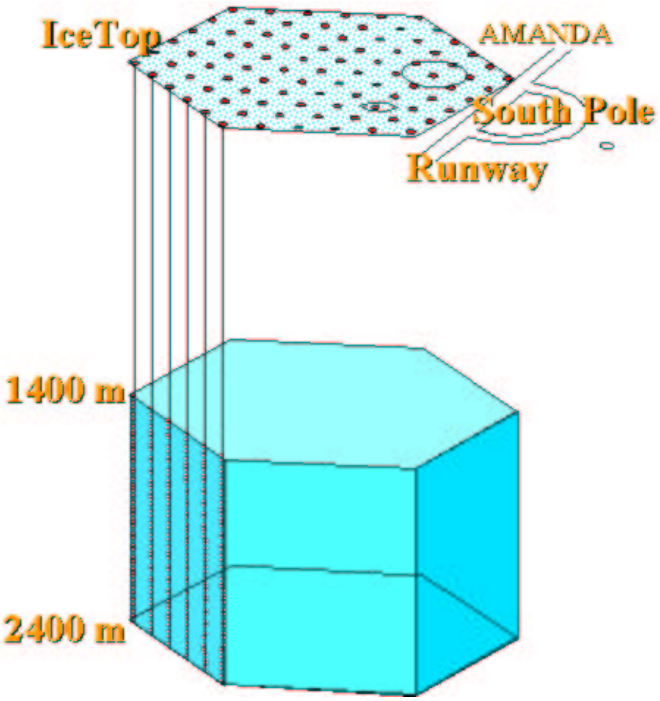

Figure 1.4: DOM arrangement in the IceCube detector. The each string has instrumented in the vertical holes of ice had 60 DOMs. They will be arranged three dimensionally.

Chapter 2

Propagation of Neutrinos and Charged Leptons

2.1 Interactions of Neutrinos and Charged Leptons

The EHE neutrinos that arrive at the earth interact with the medium in the earth as described in chapter 1. The produced neutrinos and charged leptons via NC or CC can propagate in the earth interacting with nucleons of matter around them.

The relevant interactions for EHE neutrinos are

- neutral current interaction
- charged current interaction

and that for EHE charged leptons are

- pair creation
- bremsstrahlung
- knock-on electrons
- photo-nuclear interaction

Figure 2.1 shows differential cross sections of interactions described in this section. The details of calculations are described below.

2.1.1 Neutrino Interaction

Neutrinos interact with nucleon of the propagation medium, and produced neutrinos or charged leptons via neutral current interaction (NC) or charged current interaction (CC);

$$\begin{aligned} \nu_l(\bar{\nu}_l) + N &\rightarrow \nu_l(\bar{\nu}_l) + X \quad (NC), \\ \nu_l(\bar{\nu}_l) + N &\rightarrow l^{\mp} + X \quad (CC), \end{aligned}$$

where N is a nucleon of the medium, l is charged lepton (e, μ, τ), X is produced hadrons.

For EHE neutrinos, the cross sections of those interactions depend on the behavior of parton distributions at very small values of the momentum fraction, however, where there are no direct experimental measurement. So we used the cross sections calculated by CTEQ [3, 4].

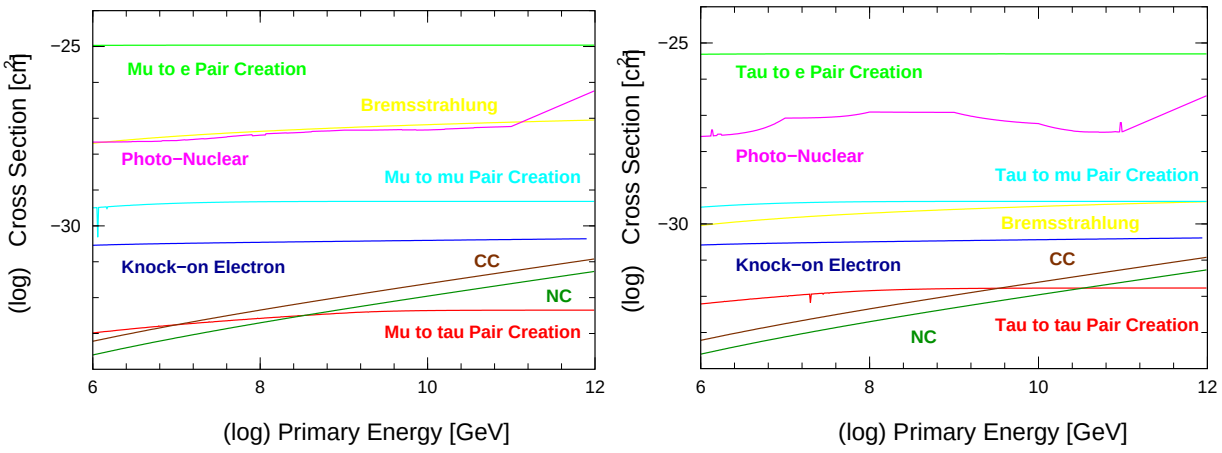

Figure 2.1: The left panel shows the cross sections in ice for ν_μ and μ. The right panel shows that for ν_τ and τ. The most dominant interaction is pair creation producing $e^\pm$ pair. The photo-nuclear cross section has large uncertainty from its parameterization.

2.1.2 Charged Lepton Interaction

Pair Creation

When high energy charged leptons (μ and τ) interact with an nucleon of the propagation medium, a pair of the $e^\pm$ or $\mu^\pm$ or $\tau^\pm$ is produced. The pair creation of an $e^\pm$ pair is dominant.

We define the inelasticity y as

$$y = 1 - \frac{E_{rec}}{E_{in}} = \frac{E_{pro}}{E_{in}}, \tag{2.1}$$

where E_{rec} is the energy of recoiling charged lepton, E_{in} is that of incoming charged leptons and E_{pro} is that of a produced pair ($e^\pm$ or $\mu^\pm$ or $\tau^\pm$).

The differential cross section is calculated as Ref. [6];

$$\frac{d\sigma_{pairC}}{dy}(E_{in}, y) = \alpha^2 R_e^2 Z \left(Z + \zeta(E_{in}, Z)\right) \frac{m_e}{m_{pro}} \frac{2}{3\pi} \frac{1-y}{y} \int_\rho \left[\phi_{pro} + \left(\frac{m_{pro}}{m_{in}}\right)^2 \phi_{rec}\right] d\rho \tag{2.2}$$

where α is the structure constant, R_e is the classical electron radius and Z is the charge of propagation medium. The $\zeta(E_{in}, Z)$ is the correction factor for screening effect on an atomic electron. It is parametrized as

$$\zeta(E_{in}, Z) = \begin{cases} 0 & E \geq 35 m_{in} \\ 0.073 \ln \dfrac{E_{in}/m_{in}}{1 + \gamma_1 Z^{2/3} E_{in}/m_{in}} & \text{otherwise} \\ 0.058 \ln \dfrac{E_{in}/m_{in}}{1 + \gamma_2 Z^{1/3} E_{in}/m_{in}} & \end{cases} \tag{2.3}$$

$$\gamma_1 = \begin{cases} 4.4 \times 10^{-5} & \text{for Hydrogen} \\ 1.95 \times 10^{-5} & \text{otherwise} \end{cases}$$

$$\gamma_2 = \begin{cases} 4.8 \times 10^{-5} & \text{for Hydrogen} \\ 5.30 \times 10^{-5} & \text{otherwise.} \end{cases}$$

The ratio of electron mass and produced particle's mass, m_e/m_{pro} is the scaling factor for the flavor of produced particles.

The last term integraled over ρ is an asymmetry term, it is defined by

$$\rho = \frac{E^+ - E^-}{E^+ + E^-}, \quad |\rho| \leq \left(1 - \frac{6m_{in}^2}{E_{in}^2(1-y)}\right)\sqrt{1 - \frac{4m_{pro}}{E_{in}y}}, \tag{2.4}$$

where E^+, E^- is the energy of produced l^+, l^-, respectively.

The functions ϕ_{pro} and ϕ_{rec} is defined as

$$\phi_{pro} = \left\{ \left[(2+\rho^2)(1+\beta) + \xi(3+\rho^3)\right] \ln\left(1 + \frac{1}{\xi}\right) + \frac{1-\rho^2-\beta}{1+\xi} - (3+\rho^2) \right\} L_{pro}, \tag{2.5}$$

$$\begin{aligned} \phi_{rec} = \Bigg\{ & \left[(1+\rho^2)(1+\frac{3}{2}\beta) - \frac{(1-\rho^2)(1+2\beta)}{\xi}\right] \ln(1+\xi) \\ & + \frac{\xi(1-\rho^2-\beta)}{1+\xi} + (1-\rho^2)(1+2\beta) \Bigg\} L_{rec}, \end{aligned} \tag{2.6}$$

$$\begin{aligned} L_{pro} = & \ln\left[\frac{RZ^{-1/3}\sqrt{(1+\xi)(1+Y_{pro})}}{1 + \dfrac{2m_{rec}\sqrt{e}RZ^{-1/3}(1+\xi)(1+Y_{pro})}{E_{in}y(1-\rho^2)}}\right] \\ & + \frac{1}{2}\ln\left[1 + \left(\frac{3m_{pro}}{2m_{in}}Z^{1/3}\right)^2 (1+\xi)(1+Y_{pro})\right], \end{aligned} \tag{2.7}$$

$$L_{rec} = \ln\left[\frac{\dfrac{3m_{pro}}{2m_{in}}Z^{1/3}}{1 + \dfrac{2m_{rec}\sqrt{e}RZ^{-1/3}(1+\xi)(1+Y_{pro})}{E_{in}y(1-\rho^2)}}\right], \tag{2.8}$$

$$Y_{rec} = \frac{5 - \rho^2 + 4\beta(1+\rho^2)}{2(1+3\beta)\ln(3+1/\xi) - \rho^2 - 2\beta(2-\rho^2)}, \tag{2.9}$$

$$Y_{pro} = \frac{4 + \rho^2 + 3\beta(1+\rho^2)}{(1+\rho^2)(3/2+2\beta)\ln(3+\xi) + 1 - 3\rho^2/2}, \tag{2.10}$$

$$\beta = \frac{y^2}{2(1-y)}, \qquad \xi = \left(\frac{m_{in}y}{2m_{pro}}\right)^2 \frac{1-\rho^2}{1-y},$$

where R is the radiation constant, and e is the base of natural logarithm. The integration limits for pair creation is given by

$$y_{min} = \frac{4m_{pro}}{E_{in}}, \qquad y_{max} = 1 - \frac{3}{4}\sqrt{e}\frac{m_{in}}{E_{in}}Z^{1/3}. \tag{2.11}$$

Bremsstrahlung

When charged leptons interact with the electromagnetic field produced by atoms of the propagation medium, an emitted high energy photon induced electromagnetic cascade. The differential cross section of bremsstrahlung is parametrized as Ref. [10];

$$\frac{d\sigma_{bremss}}{dy}(E_{in}, y) = 4\alpha R_e^2 Z^2 \left(\frac{m_{in}}{m_{pro}}\right)^2 \frac{1}{y}\left\{(2 - 2y + y^2)\Psi_1(q_{min}, Z) - \frac{2}{3}(1-y)\Psi_2(q_{min}, Z)\right\}, \tag{2.12}$$

where the functions $\Psi_1(q_{min}, Z)$ and $\Psi_2(q_{min}, Z)$ is defined by

$$\Psi_{1,2}(q_{min}, Z) = \Psi^0_{1,2}(q_{min}, Z) - \Delta_{1,2}(q_{min}, Z), \tag{2.13}$$

$$\Psi^0_1(q_{min}, Z) = \frac{1}{2}\left(1 + \ln\frac{m_{in}^2 a_1^2}{1+x_1^2}\right) - x_1 \arctan\frac{1}{x_1} + \frac{1}{Z}\left[\frac{1}{2}\left(1 + \ln\frac{m_{in}^2 a_2^2}{1+x_2^2}\right) - x_2 \arctan\frac{1}{x_2}\right], \tag{2.14}$$

$$\begin{aligned}\Psi^0_2(q_{min}, Z) = {} & \frac{1}{2}\left(\frac{2}{3} + \ln\frac{m_{in}^2 a_1^2}{1+x_1^2}\right) + 2x_1^2\left(1 - x_1 \arctan\frac{1}{x_1} + \frac{3}{4}\ln\frac{x_1^2}{1+x_1^2}\right) \\ & + \frac{1}{Z}\left[\frac{1}{2}\left(\frac{2}{3} + \ln\frac{m_{in}^2 a_2^2}{1+x_2^2}\right) + 2x_2^2\left(1 - x_2 \arctan\frac{1}{x_2} + \frac{3}{4}\ln\frac{x_2^2}{1+x_2^2}\right)\right],\end{aligned} \tag{2.15}$$

$$\Delta_1(q_{min}, Z) = \begin{cases} 0 & (Z = 0) \\ \ln\dfrac{m_{in}}{q_c} + \dfrac{\zeta}{2}\ln\dfrac{\zeta+1}{\zeta-1} & (Z \neq 0), \end{cases}$$

$$\Delta_2(q_{min}, Z) = \begin{cases} 0 & (Z = 0) \\ \ln\dfrac{m_{in}}{q_c} + \dfrac{\zeta}{4}(3-\zeta^2)\ln\dfrac{\zeta+1}{\zeta-1} + \dfrac{m_{in}^2}{q_c^2} & (Z \neq 0), \end{cases}$$

$$q_{min} = \frac{m_{in}^2 y}{2E_{in}(1-y)}, \quad x_i = a_i q_{min} \ \ (i = 1, 2), \quad a_1 = \frac{111.7}{Z^{1/3}m_{pro}}, \quad a_2 = \frac{724.2}{Z^{2/3}m_{pro}},$$

$$\zeta = \sqrt{1 + \frac{4m_{in}^2}{q_c^2}}, \quad q_c = \frac{1.9 m_{in}}{Z^{1/3}}.$$

The integration limits for bremsstrahlung is given by

$$y_{min} = 0, \qquad y_{max} = 1 - \frac{3}{4}\sqrt{e}\frac{m_{in}}{E_{in}}Z^{1/3}. \tag{2.16}$$

Knock-On Electrons

The charged leptons also can "knock on" the atomic electrons of propagation medium. The differential cross section of knock-on electrons is parametrized as Ref. [10];

$$\frac{d\sigma_{knock}}{dy}(E_{in}, y) = 2\pi R_e^2 Z \frac{m_{pro}}{\beta^2 E}\left(\frac{1}{y^2} - \frac{1}{y}\frac{\beta^2}{y_{max}} + \frac{1}{2}\right)(1 + \Delta(E_{in}, y)), \tag{2.17}$$

$$\Delta(E_{in}, y) = \frac{\alpha}{2\pi}\ln\left(1 + \frac{2yE_{in}}{m_{pro}}\right)\left[\ln\left(\frac{4E_{in}^2(1-y)}{m_{in}^2}\right) - \ln\left(1 + \frac{2yE_{in}}{m_{pro}}\right)\right] \tag{2.18}$$

where $\beta = p/E_{in}$, p is the four momentum of the incoming charged lepton, and y_{max} is the upper limit of integration. The integration limits for knock-on electrons is given by

$$y_{min} = \frac{\bar{I}}{E_{in}}, \qquad y_{max} = \frac{2m_{pro}\beta^2 E_{in}}{m_{pro}^2 + m_{in}^2 + 2m_{pro}E_{in}}. \tag{2.19}$$

where $\bar{I}$ is the mean of ionization potential of the propagation medium.

Photo-nuclear Interaction

The photo-nuclear is the interaction of charged lepton with nuclei via virtual photon. The photo-nuclear cross section is calculated using the deep-inelastic scattering formalism with the ALLM parametrization for the nucleon structure function [13, 14].

The photo-nuclear interaction is described as

$$l(k_{in})N(p) \to l(k_{rec})X,$$

where l is a charged lepton, and k_{in}, k_{rec} is the four momentum of incoming and recoiling charged lepton, respectively. The N is nucleon, and X is hadron changed via interaction. The X induces the hadronic cascade.

The variables used in the calculations are defined as

$$q^2 = (k_{in} - k_{rec})^2 = -Q^2, \tag{2.20}$$

$$x = \frac{Q^2}{2p \cdot q} \tag{2.21}$$

$$y = \frac{p \cdot q}{p \cdot k_{in}}. \tag{2.22}$$

The differential cross section of photo-nuclear interaction is given by

$$\frac{d\sigma_{photo}}{dQ^2 dx} = \frac{4\pi\alpha^2}{Q^2 x}\left[1 - y - \frac{Q^2}{4E_{in}} + \left(1 - \frac{2m_{in}}{Q^2}\right)\frac{y^2}{2}\left(1 + \frac{4M_p^2 x^2}{Q^2}\right)\right] F_N(x, Q^2) \tag{2.23}$$

where M_p is the proton mass, m_{in} is the incoming particle mass and E_{in} is the incoming particle energy. The nucleon structure function is given by Ref. [13];

$$F_N(x,Q^2) = a(A,x)F_P(x,Q^2)(Z+(A-Z)P(x)), \tag{2.24}$$

$$P(x) = 1-1.85x+2.45x^2+2.35x^3+x^4. \tag{2.25}$$

The $F_P(x,Q^2)$ is the proton structure function parametrized by ALLM97 [14]. It is given by

$$F_P(x,Q^2) = \frac{Q^2}{Q^2+m_0^2}\left(F^P(x,Q^2)+F^R(x,Q^2)\right), \tag{2.26}$$

$$F^P(x,Q^2) = c_P(t)x_P^{a_P(t)}(1-x)^{b_P(t)}, \tag{2.27}$$

$$F^R(x,Q^2) = c_R(t)x_R^{a_R(t)}(1-x)^{b_R(t)}. \tag{2.28}$$

where x_P and x_R are defined by

$$x_P = \left(1+\frac{W^2-M_p^2}{Q^2+m_P^2}\right)^{-1}, \tag{2.29}$$

$$x_R = \left(1+\frac{W^2-M_p^2}{Q^2+m_R^2}\right)^{-1}. \tag{2.30}$$

where W^2 is the center of mass energy (GeV^2), m_P^2 and m_R^2 are given by Table 2.1.

The parameters in (2.27) and (2.28) is defined as functions of t;

$$t = \ln\left(\frac{\ln\frac{Q^2+Q_0^2}{\Lambda^2}}{\ln\frac{Q_0^2}{\Lambda^2}}\right) \tag{2.31}$$

where Q_0 and Λ are given by Table 2.1. Some of the parameters which is the function of t; $a_R(t)$, $b_R(t)$, $c_R(t)$ and $b_P(t)$ is given by

$$f(t) = f_1+f_2t^{f_3}, \tag{2.32}$$

while $a_P(t)$ and $c_P(t)$ are given by

$$g(t) = g_1+(g_1-g_2)\left(\frac{1}{1+t^{g_3}}-1\right). \tag{2.33}$$

The parameters in (2.32) and (2.33) (c_{P1}, c_{P2} etc.) are also given by Table 2.1.

The $a(A,x)$ in (2.24) is the ratio of the nuclear structure function to that of nucleon. It is given by

$$a(A,x) = \begin{cases} A^{-0.1} & x \le 0.0014 \\ A^{0.069\log_{10}x+0.097} & 0.0014 < x \le 0.04 \\ 1 & 0.04 < x. \end{cases} \tag{2.34}$$

m_0^2 GeV^2	0.31985	b_{P1}	0.60243
m_P^2 GeV^2	49.457	b_{P2}	1.3754
m_R^2 GeV^2	0.15052	b_{P3}	1.8439
Q_0^2 GeV^2	0.46017	c_{R1}	0.80107
Λ^2 GeV^2	0.06527	c_{R2}	0.97307
c_{P1}	0.28067	c_{R3}	3.4942
c_{P2}	0.22291	a_{R1}	0.58400
c_{P3}	2.1979	a_{R2}	0.37888
a_{P1}	-0.0808	a_{R3}	2.6063
a_{P2}	-0.44812	b_{R1}	0.10711
a_{P3}	1.1709	b_{R2}	1.9386
		b_{R3}	0.49338

Table 2.1: The parameters for proton structure function by ALLM97 [14].

The differential cross section $d\sigma/dy$ is given by integration of $d\sigma/dQ^2dx$ over dQ^2 using valiable transformation from x to y. The valiable x and y are related by

$$x = \frac{Q^2}{2M_pE_{in}y}, \tag{2.35}$$

$$dx = \frac{Q^2}{2M_pE_{in}y^2}\, dy. \tag{2.36}$$

The differential cross section is given by

$$\frac{d\sigma}{dy} = \int dQ^2 \frac{d\sigma}{dxdQ^2}\frac{dx}{dy}. \tag{2.37}$$

2.2 Decays of Charged Leptons

The μ decay and τ to lepton decay is calculated using the approximation that produced lepton mass is negligible compared to parent lepton mass [11]. The differential decay rate is given by

$$\frac{dn}{dy_\nu} = 2 - 6y_\nu + 4y_\nu^3 - (-2 + 12y_\nu - 18y_\nu^2 + 8y_\nu^3), \tag{2.38}$$

where $y_\nu = E_{\nu_e}/E_{\nu_\mu}$ (for μ decay), $E_{\nu_{e,\mu}}/E_{\nu_\tau}$ (for τ decay), and

$$\frac{dn}{dz_l} = \frac{5}{3} - 3z_l^2 + \frac{4}{3}z_l^3 - (\frac{1}{3} - 3z_l^2 + \frac{8}{3}z_l^3), \tag{2.39}$$

where $z_l = E_{\nu_l}/E_l$, l is charged lepton (μ or τ).

The distribution of τ to hadron decay is given by

$$\frac{dn}{dz} = \sum_i B_i \frac{1}{1 - r_i}, \qquad r_i = \frac{m_i^2}{m_\tau^2} \tag{2.40}$$

where i indicates produced hadrons such as π, ρ, a_1, and X(other hadrons). The B_i is the branching ratio of the each decay mode which is normalized by

$$\int \frac{dn}{dz} dz = \sum_i B_i = 1. \tag{2.41}$$

2.3 Issues and Motivation

The accurate understanding of the EHE particles propagation in the earth is essential to search for EHE cosmic neutrinos by an underground neutrino telescope. Let me explain why.

In the case of EHE particles, because the chain reactions of the interactions and decays occur during the propagation in the earth, *e.g.,* $\nu_\mu \xrightarrow{CC} \mu \xrightarrow{PairCreation} \tau \xrightarrow{decay} \mu \cdots$, the behavior of particle propagation in EHE range is rather complex, and full calculations to follow all the interactions/decays and secondary produced particles is indispensable to estimate the detection sensitivities. Full Monte-Carlo simulator to follow all these particles may take too long time in practice, however, so we should develop the effective calculation method for saving CPU time. It should be noted that any method for particle propagation in EHE region demands a capability to treat μ's and τ's on the same footing to handle the chain reactions. Furthermore, as the particle intensity is expected to depend strongly on the nadir angle, one has to calculate the particle flux in all phase space of solid angles because the IceCube is three dimensional array with 4π detection sensitivity. The most practical way to satisfy these requirements is to build the proper transport equations and numerically resolve them.

The transport equations which describe the propagation of neutrinos and charged leptons in the earth are given by Ref. [15], using differential cross sections;

for neutrino propagation:

$$\begin{aligned}
\frac{dN_\nu}{dx dE_\nu} &= -N_A \sigma_{CC+NC}(E_l) \frac{dN_\nu}{dE_\nu} + \frac{m_l}{c\tau_l \rho} \int dE_l \frac{1}{E_l} \frac{dn_l}{dE_\nu} \frac{dN_l}{dE_l} \\
&+ N_A \int dE_l' \frac{d\sigma_{lN\cdot CC}}{dE_\nu} \frac{dN_l}{dE_l'} + N_A \int dE_\nu' \frac{d\sigma_{\nu N\cdot NC}}{dE_\nu} \frac{dN_\nu}{dE_\nu'}
\end{aligned} \tag{2.42}$$

for charged lepton propagation:

$$\begin{aligned}
\frac{dN_l}{dx dE_l} &= -N_A \sigma_{CC}(E_l) \frac{dN_l}{dE_l} - \frac{m_l}{c\tau_l \rho} \frac{1}{E_l} \frac{dN_l}{dE_l} \\
&+ \frac{m_l}{c\tau_l \rho} \int dE_l' \frac{1}{E_l'} \frac{dn_l}{dE_l} \frac{dN_l}{dE_l'} \\
&+ N_A \int dE_\nu' \frac{d\sigma_{\nu N\cdot CC}}{dE_l} \frac{dN_\nu}{dE_\nu'} + N_A \int dE_l' \frac{d\sigma_{lN}}{dE_l} \frac{dN_l}{dE_l'}
\end{aligned} \tag{2.43}$$

where N_A is the Avogadro's number, c is the speed of light, m_l is the mass of the charged lepton l, τ_l is the lifetime of the l, x is the column density, unit in [g/cm^2], which is defined by

$$x \equiv \int_0^R \rho(r) dr. \tag{2.44}$$

The $\rho(r)$ is the density of the propagation medium, which depends on particle location.

The first term of eq.(2.42) indicates the neutrino reduction due to the CC and NC. The second term indicates the neutrino appearance due to the lepton decay. The third and fourth terms indicate the neutrino appearance due to the CC and NC, respectively. The $d\sigma_{lN\cdot CC}/dE_\nu$ term represents that the energy interactions of the charged lepton l (due to the pair creation, bremsstrahlung, etc.) should be taken account.

The first and second terms of eq.(2.43) represent the charged lepton reduction due to the CC and decay, respectively. The third term indicates the appearance of charged lepton due to the lepton decay. The fourth term represents the neutrino appearance due to the CC. The last term accounts the interactions such as pair creation, bremsstrahlung etc.

We need the numerical simulator which can solve the transport equations (eq.(2.42) and (2.43)) for the long distance and for the all solid angles with saving CPU time.

The IceCube does not directly measure the energy of the EHE particle, but the energy deposit in the detector. The energy deposit of an EHE particle are given by

$$-\frac{dE}{dx} = \alpha + \beta E \tag{2.45}$$

$$\simeq \beta E \tag{2.46}$$

$$= \left(\int y \frac{d\sigma}{dy} dy \right) E, \tag{2.47}$$

where the α is the ionization continuous loss term and β is the stochastic energy loss term by other interactions such as pair creation, bremsstrahlung, knock-on electrons, and photo-nuclear interactions. The β depends on weakly the particle's energy, E. The β term is dominant for EHE particles. In order to understand the stochastic energy deposit in the detector, we should handle it as probability distribution by using the Monte-Carlo method. The Monte-Carlo method is the technique to sample a variable following a given probability distribution using the random number. The relation between the random number r and the probability distribution $f(x)$ is given by

$$r = F(x) = \int_{-\infty}^{x} f(t)dt, \qquad \int f(x)dx = 1.$$

By sorting the $F(x)$, the uniform random number r samples a value of x.

In order to understand *both* the EHE particles propagation in the earth and in the detector, we developed the simulator which can calculate propagation in the earth numerically, and the energy deposit in the detector by the Monte-Carlo method.

Chapter 3

Development of Java-based MonteCarlo/Numerical Simulator

3.1 Design Policy

We developed Java-based Monte-Carlo/Numerical simulator named **JULIeT** $\sim$ **Java-based Ultra high energy Leptons IntEgral Transportor**. In order to solve the issues described in section 2.3, the JULIeT must meet a couple of requirements.

The first requirement is that the JULIeT should be able to trace neutrinos and charged leptons propagating in the earth by solving the transport equations (eq.(2.42) and eq.(2.43)) numerically. Therefore the JULIeT is designed to solve the transport equations and produce the matrices describing the particle propagation in the earth in order to obtain the fluxes of the particles arrived at the detector depth with all the solid angle. The second requirement is that the JULIeT should be also able to trace particles in the detector *i.e.* in ice by Monte-Carlo method in order to obtain the distribution of the energy deposit as electromagnetic and hadronic cascades produced in the detector.

The JULIeT is designed to have capability of calculating the IceCube sensitivity on EHE neutrino detection with reasonable CPU time (chapter 3).

We introduced Java technology, one of the most modern programing languages, because

- the Java is the object-oriented programming language which makes it easy to build large source codes and update them over long years,
- amount of source codes can be shorter than that in C++,
- it provides an OS-independent platform.

3.2 Structure of JULIeT

The JULIeT is based on a package system. Each package contains classes under similar concepts. Fig.3.1 shows the structure of the packages. The details of the roles of each packages and their classes are described below.

Table.3.1 shows the first order interactions/decays channels considered in the JULIeT. The details of each interactions/decays channels are described in section 2.1 and 2.2. The particles handled in the JULIeT

Table 3.1: Channels of infinitesimal propagation.
Rows are primary and columns are produced/survival particles.

	ν_e	ν_μ	ν_τ	e/γ	μ	τ	hadron
ν_e	NC[a]/S[h]			CC[b]			NC/CC
ν_μ		NC/S			CC		NC/CC
ν_τ			NC/S			CC	NC/CC
μ	D[c]	CC/D		PC[d]/B[e]/K[f]/D	PC/S	PC	NC/CC/PN[g]
τ	D	D	CC/D	PC/B/K/D	PC/D	PC/S	NC/CC/D

[a]Neutral Current interaction
[b]Charged Current interaction
[c]Decay
[d]Pair Creation
[e]Bremsstrahlung
[f]Knock-on Electron
[g]Photo-nuclear interaction
[h]Survive

are ν_e, ν_μ, ν_τ, μ and τ. Allowed region of primary energy of particles is from 10^6[GeV] to 10^{12}[GeV], and that of produced energy of particles is from 10^2[GeV] to 10^{12}[GeV].

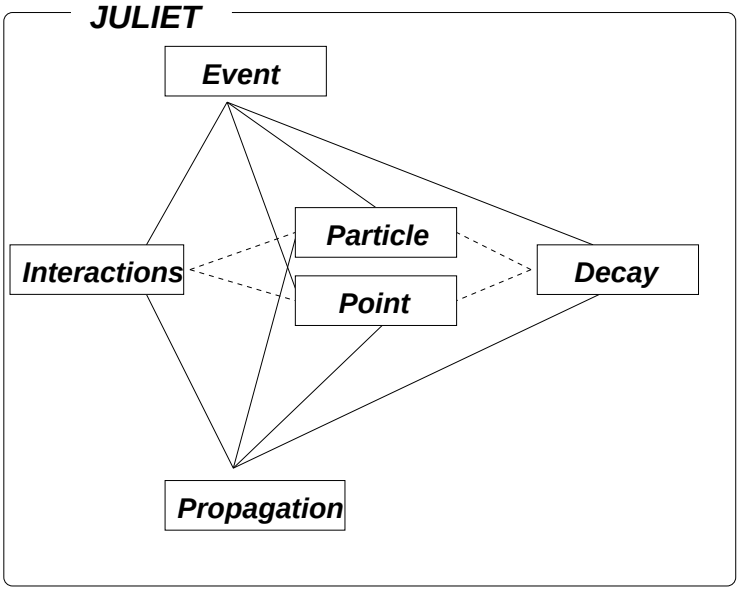

Figure 3.1: Package Structure of the JULIeT.

The representative packages among them are propagation and event both of which has its own method to run the simulation. The propagation package contains the classes to calculate the particle propagation by numerically solving the relevant transport equations (eq.(2.42) and eq.(2.43)). The event package is a group of the classes to calculate the particle propagation with Monte-Carlo methods. It has the interactive

mode to run the simulation. The propagation and event packages rely on classes in all the other packages, such as the interaction package which is responsible for handling the particle interactions. The relation between the classes are shown in Figure 3.2 for the propagation package, and Figure 3.3 for the event package.

3.2.1 Points Package

This package contains the classes concerning the particle location and the propagation medium. The class in this package, ParticlePoint class, provides the point vector used by calculations on propagation of EHE particles in the earth. Figure 3.4 shows the definition of geometric parameters. It also provides the parameters of the medium such as the density which are used for the calculations of differential cross sections.

3.2.2 Particles Package

This package contains the Particle class to define particles and their property such as their mass, name, flavor, doublet, and lifetime. It also provides their energy.

3.2.3 Interactions Package

This package contains the classes to define interactions such as PairCreation class, Bremsstrahlung class etc. They are classes inherit from Interactions class. It also has the classes (MakeBremsstrahlungMtx class etc.) to make dumped matrices which elements are differential cross sections corresponding to log-energy of primary and produced particles. The dumped matrices defined in InteractionsMatrix class are "serialized" objects, which provide "get" methods to return the differential/total cross sections, particle's flavor, doublet, energy and so on. The differential cross sections are calculated as described in section 2.1. The matrices made in this package are used by calculations of propagation in the earth.

Additionally, this package has InteractionsBase class and ElectronBase class which are extended from its super class, MonteCarloBase class in event package (See 3.2.6). These "Base" classes exist in order that classes in event package which calculate the particle propagation by Monte-Carlo method can handle all of the interactions/decays under the same footing. These classes essentially provide the probability tables to sample the pathlength of interaction and produced energy with Monte-Carlo methods (See 3.2.6). It also supplies the method to return the pathlength and produced energy for a given random number.

3.2.4 Decay Package

The classes in this package handle the lepton decay processes such as $\tau \rightarrow \mu \rightarrow$e, and make decay matrices which elements are differential decay rate.

The Tau(Mu)DecayYMatrix class are similar with the InteractionsMatrix class in the interaction package. These classes make the matrices of the energy transfer $dN/dLogy$ for the decays. The matrix elements are calculated by the methods supplied by the Decay class. The decay rates are calculated as described in section 2.2. The biggest difference between Tau(Mu)DecayYMatrix class and InteractionsMatrix class is, the decay matrix element is calculated whenever the object is generated while interaction matrices are usually pre-calculated and stored in form of files to be read out for the Event/PropagationMatrix class. This is because it takes much less time to calculate the decay matrices than the interaction matrices.

There are also "Base" classes, MuDecayBase and TauDecayBase, for calculations of the particle propagation by Monte-Carlo methods. Similar with the InteractionsBase class, they calculate the Monte-Carlo

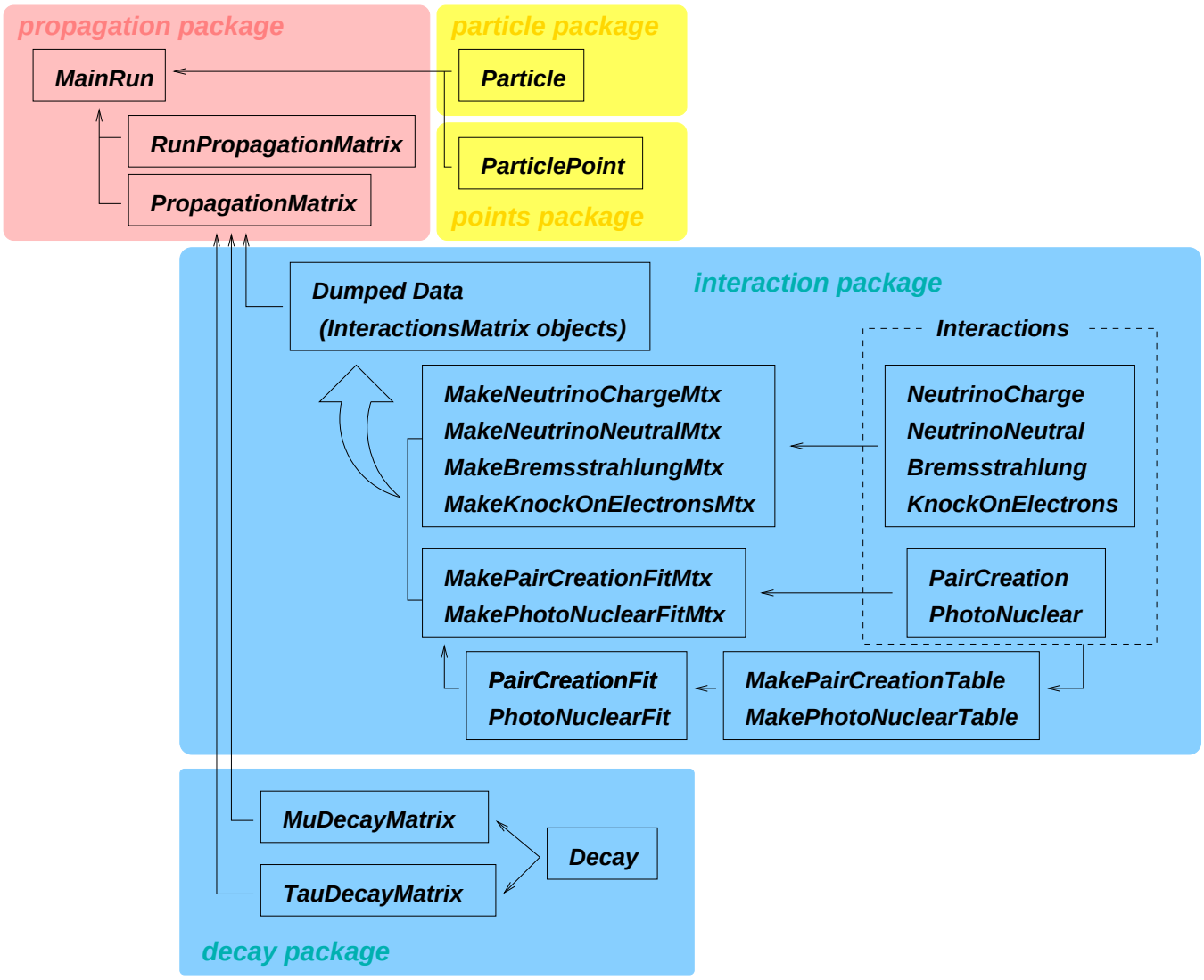

Figure 3.2: Class structure of the JULIeT from aspects of the Propagation package. MainRun class has a main program for tracing neutrinos and charged leptons in the earth.

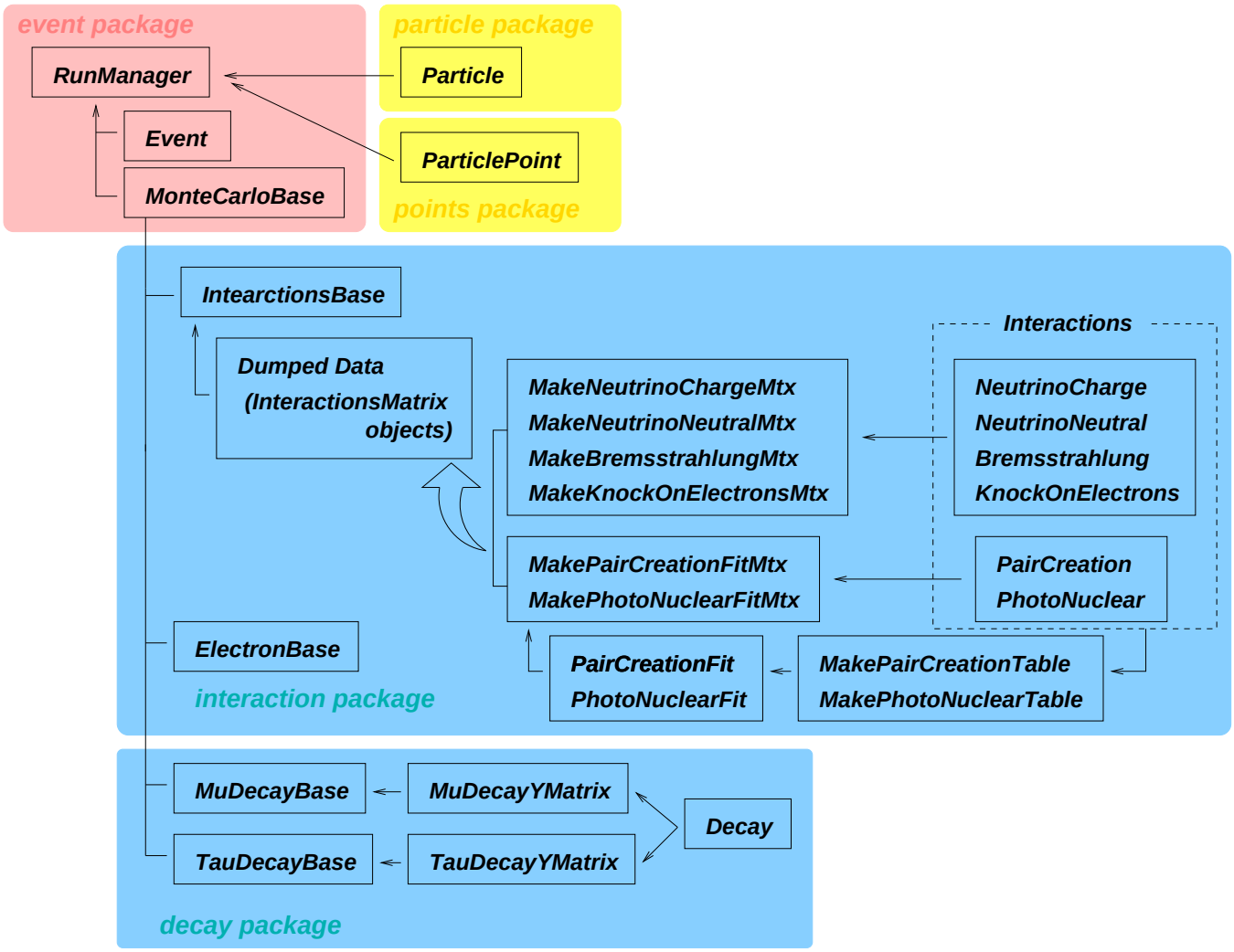

Figure 3.3: Class structure of the JULIeT from aspects of the event package. RunManager class has a main program for tracing neutrinos and charged leptons in the IceCube detection volume.

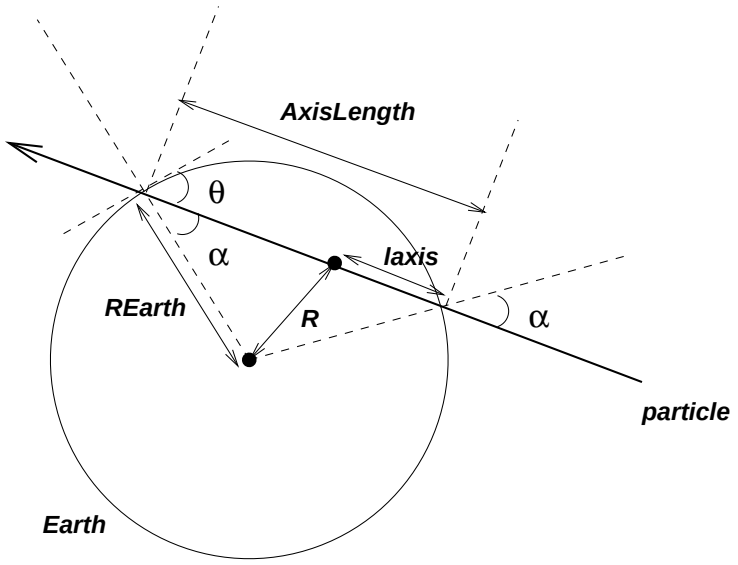

Figure 3.4: Definition of geometric parameters. The α is nadia angle, θ is zenith angle.

probability table using the decay matrices calculated by the MuDecayYMatix class and TauDecayYMatrix class.

The τ decay has some decay modes such as $\tau \to \mu$, e, and hadrons. The branching ratio of each mode are supplied in the Decay class. The hadrons produced via τdecay may be π, ρ and so on. But we regard them as a hypothetical 'hadron' which is made of superpositions of π, ρ and so on.

The mode of τ decay is determined by the method supplied in TauDecayBase class. In the method, a cumulative table of branching ratio is produced, and one of the decay mode is chosen by random number.

3.2.5 Propagation Package

This package contains the classes for numerically solving the transport equations (eq.(2.42) and eq.(2.43)), which provides a faster and more accurate evaluation of the particle propagation in long distances.

The propagation matrices calculated in this package describe the energy and particle species transfer by the interactions/decays. They are built by pre-calculated InteractionsMatrix and MuDecayYMatix/TauDecayYMatrix objects. The elements of the matrices indicate the energy distribution and the flux of particles after propagation of an infinitesimal distance in the earth. In this package, there is the MainRun class which has a main method to calculate the propagation matrices.

The procedure of making propagation matrices is described below. Figure 3.2 shows the relation between the classes in this package.

Calculation of the propagation matrices:

1) In order to avoid sizable error due to the rock density profile, the trajectory length is divided to 5 sections.
2) The following calculations **3) ∼7)** is repeated 5 times (for each section).
3) The elementary infinitesimal propagation matrices over infinitesimal distance ($dX[g/cm^2]$) are built using differential cross sections calculated in the interactions package.
4) The particles are propagated over $X = 10 \times dX[g/cm^2]$, *i.e.* infinitesimal propagation matrices

produced in **3)** is multiplied 10 times.

5) The particles are propagated over $X \times 2^k [g/cm^2]$, where k is the number of steps needed to propagate the section, *i.e.* finite propagation matrix produced in **5)** is multiplied 2^k times.

6) During **5)**, the matrices are stored when particles reaches 3 % of the total path in their journey.

7) After **5)**, the resultant matrices propagated over the section are stored.

8) For a rest of trajectory length, particles are propagated by multiple the matrix stored in **5)** until the particles reach the final point.

3.2.6 Event Package

This package contains the classes related to 'occurrence of event'. These classes define the behavior of an event for propagating particles by Monte Carlo methods.

There is the MonteCarloBase class in this package. It is a super class of InteractionsBase and ElectronBase which are classes in the interactions package and MuDecayBase and TauDecayBase which are classes in the decay package. The Event class and RunManager class handle the interactions/decays in form of "list". In order to register interactions and decays in the list, all the interactions/decays should have a common super class. The MonteCarloBase class is an abstract class defines the methods for both interactions and decay that determines the pathlength and produced energy with the Monte-Carlo methods. The actual implements of the methods are made by each "Base" class. It also defines methods to get the information of interactions/decays so that the Event class can know that information.

The Event class actually makes an event. It is the fundamental class for propagating particles by the Monte-Carlo methods. Table 3.2 shows channels of the interaction/decay considered in the Monte-Carlo methods. The CC interaction from charged lepton to neutrino is negligible because propagation distance (detector size) is short enough. The neutrinos produced via charged lepton decay are also neglected by the same reason. In order to save CPU time, the differential cross sections of these interactions are pre-calculated by MakeBremsstrahlungMtx class etc. in Interactions package. An interaction/decay which returns the shortest pathlength is chosen, and an "event" has occurred then particles propagate. So the information of an interaction/decay which has occurred, such as transfered energy, produced particle, pathlength *etc.* are supplied the methods of Event class.

The procedure of choosing an interaction/decay which returns the shortest pathlength, and choosing the produced energy via the interaction/decay by Monte-Carlo method are described below. Figure 3.3 shows the relation between the classes in this package.

Calculation of the pathlength by the Monte-Carlo method:

a) In the case of the changed lepton interactions

The number of particles when they propagate X[g/cm^2] is given by

$$\frac{dN}{dX} = -\sigma(E)N, \tag{3.1}$$

$$N(E,X) = N(E,X_0)\ \exp[-(X-X_0)N_A\ \sigma(E)], \tag{3.2}$$

where N_A is the Avogadro's number. The probability that interaction has occurred while a particle propagates X[g/cm^2] is given by

$$P(E,X) = 1-\exp[-XN_A\ \sigma(E)]. \tag{3.3}$$

Table 3.2: Channels of interaction/decay for Monte-Carlo simulation. Rows are primary and columns are produced particles. The CC interaction from charged lepton to neutrino is negligible for a propagation distance (detector size) considered here. The neutrinos produced via charged lepton decay are also neglected by the same reason.

	ν_e	ν_μ	ν_τ	e/γ	μ	τ	hadron
ν_e	NC[a]			CC[b]			NC/CC
ν_μ		NC					NC/CC
ν_τ			NC				NC/C
μ				PC[d]/B[e]/K[f]/D	PC	PC	PN[g]
τ				PC/B/K/D	PC/D[c]	PC	D

[a]Neutral Current interaction
[b]Charged Current interaction
[c]Decay
[d]Pair Creation
[e]Bremsstrahlung
[f]Knock-on Electron
[g]Photo-nuclear interaction
[h]Survive

The P(E,X) is determined by a random number(0∼1). So the pathlength is

$$X = \frac{-1}{N_A\ \sigma(E)}\ \ln(1-r), \tag{3.4}$$

where r is a random number.

b) In the case of the neutrino interactions

The probability that interaction has occurred while a neutrino propagates X[g/cm^2] is given by

$$P(E,X) = 1-\exp[-XN_A\ \sigma(E)] \tag{3.5}$$

$$\simeq XN_A\ \sigma(E), \tag{3.6}$$

where under an approximation that cross section of neutrino interaction is very small.
The P(E,X) is determined by random number(0∼1). So the pathlength is

$$X = \frac{r}{N_A\ \sigma(E)}, \tag{3.7}$$

where r is random number.

c) In the case of decay

The number of particles when they propagate while t[sec] is given by

$$\frac{dN}{dt} = -\frac{1}{\tau(E)}N(t), \tag{3.8}$$

$$N(E,t) = N(t_0)\ \exp\Big[-\frac{t}{\tau(E)}\Big], \tag{3.9}$$

where τ is the lifetime of the particle. The probability that decay has occurred while a particle propagates t[sec] is given by

$$P(E,t) = 1 - \exp\Big[-\frac{t}{\tau(E)}\Big]. \tag{3.10}$$

From $X = c\tau\rho$ (c is light speed and ρ is the density of the medium[g/cm^3]),

$$P(E,X) = 1 - \exp\Big[-\frac{X}{c\tau(E)\rho}\Big]. \tag{3.11}$$

The P(E,X) is determined by random number(0$\sim$1). So the pathlength is

$$X = -c\tau(E)\rho\ \ln(1-r), \tag{3.12}$$

where r is random number.

Calculation of the Produced Energy by the Monte-Carlo method:

The produced particle's energy is determined by Monte-Carlo method. Energy deposit and dimensionless energy $y = E_{pro}/E_{in}$ are related by eq.(2.47). A y is sampled using a random number by

$$r = \frac{1}{\sigma}\int \frac{d\sigma}{dy}\,dy \tag{3.13}$$

where r is a random number.

The RunManager class controls the run, so it has a main method which runs the events and records some types of data files. It calculates the distribution of the energy deposit includes their fluctuation. It can run some types of runs for recording some types of data *e.g.,* full-text-based data which records all the profile of the propagation for debugging, binary data which records distributions of energy deposit in the detector for each registered interaction/decay, and so on. For example, one of the procedure of controling the run which records binary data of the distributions of the energy deposit to electromagnetic and hadronic cascades, respectively, with given monocromatic primary energy, is described below;

Procedure of the run:

1) The constructor of the RunManager class generates a list of MonteCarloBase object whose elements are "Base" classes for each interaction/decay registered by an user interactively.
2) A Particle object is generated as a primary particle (See 3.2.2).
3) A ParticlePoint object is generated with given material(ice or rock) as a starting point (See 3.2.1).
4) An Event object is generated (See above).
5) The pathlength of interactions/decays in the list generated in the constructor is sampled and

compared with each other, then an interaction/decay which returned the shortest pathlength is determined

to take place.

6) The particle is propagated over the pathlength determined in 5).

7) If the propagating particle is still in the detector, calculations is continued.

8) The energy of the produced particle is sampled by Monte-Carlo method (See above).

9) The procedure **5) ∼ 9)** is repeated until the particle stops or changes into an electron(photon)/hadron or passes through the detector.

10) The distributions of energy deposit as electromagnetic/hadronic cascades and total energy deposit are recorded during the procedure of **2) ∼ 10)**

The simulated results calculated in this RunManager class by Monte-Carlo methods will be shown in section 3.3.

3.3 Simulated Results

As described in section 3.2, the RunManager class in the event package can calculate the particle propagation with the Monte-Carlo methods.

We ran the particles 1km in the ice, and calculated the distribution of energy deposit of them. The produced particles via interactions/decays induce electromagnetic or hadronic cascades. The resultant distributions are compared to analytic calculations.

Figure 3.5 and 3.6 shows the distribution of energy deposit for muon propagating in 1km ice (the density of the ice is $\rho = 0.917$). The energy of primary muon is 10EeV ($= 10^{10}$GeV). The analytic mean value of energy deposit in Figure 3.5 is given by

$$\left\langle -\frac{\Delta E}{E} \right\rangle = 1 - e^{\beta x},$$

where x is the path length and β is the inelasticity defined as

$$\beta = \sum_i \beta_i, \qquad \beta_i = \int y \frac{d\sigma_i}{dy} dy, \tag{3.14}$$

where the i is the index of relevant interactions. Figure 3.5 shows the distribution of energy loss to electromagnetic and hadronic cascades, respectively. The mean value of these energy deposit is consistent with analytic calculation, but you can see the fluctuation of the energy deposit shown in Figure 3.5 is not negligible.

In order to understand causes of the fluctuation, the contribution of the $e^{\pm}$ pair creation, bremsstrahlung and photo-nuclear interaction to the energy deposit are separately shown in Figure 3.6. While the energy deposit via $e^{\pm}$ pair creation has a peak, those via bremsstrahlung and photo-nuclear interaction exhibits the divergent structure. Therefore these stochastic energy loss contribute to make the distribution wide.

While the following figures show the same as above, but for τ. Figure 3.7 shows the same as Figure 3.5, but for the case of τ propagation, the contribution from decay is larger than the case of μ, because the lifetime of τ is far short compared with that of μ. The contribution of decay can be shown in Figure 3.8. The cross section of photo-nuclear interaction has large uncertainty (See Figure 2.1), because the parameterization of cross section depends on the nuclei structure function. Therefore we may need the other parameterization for photo-nuclear interaction in this energy range for systematic investigation.

The relation between the energy deposit obtained by the Monte-Carlo simulation and analytical calculation are shown in Figure 3.9 for μ and Figure 3.10 for τ as a function of primary energy. The energy deposit of μ is larger than that of τ above 10^8 GeV region. But, below 10^8 GeV region, the contribution of τ decay increases, which make a difference between the simulated result and analytical calculation.

We can also shows the contribution of interactions which induce stochastic energy loss as follows. The average distance which particles propagated until its energy becomes $1/e$ times of the primary energy, *i.e.*, "range" is determined by Monte-Carlo simulation. Figure 3.11 shows the range for μ and τ. The blue and magenta lines indicate expected range obtained by analytic calculation (blue for the τ, magenta for the μ) $1/\beta$ by eq.(3.14). The instability of the photo-nuclear cross section adversely affects both analytic and simulated values. The green line in indicates the contribution of the τ decay. Below 10^9 GeV, the contribution of τ decay plays a dominant role on the τ propagation. You can see that the range of τ is longer than that of μ. It suggests that the detection volume of τ is larger than that of μ, *i.e.* the τ flux arrive on the detector is larger than μ flux above $\sim 10^8$ GeV. However, since the contribution of τ decay is dominant, the range of τ becomes short below $\sim 10^8$ GeV.

We have discussed the case when incoming particles are muons and taus. But the IceCube detector will occasionally see events induced by incoming neutrinos events in EHE range. We, therefore, need to investigate the case when neutrinos are incoming into the $1km^3$ volume, and producing muons and taus internally. Figure 3.12 shows the energy deposit distributions when ν_μs are incoming into the detector. The ν_μ produces μ via CC interaction, but the location where CC interaction has occurred is random. The long tail shown in Figure 3.12 reflects the difference of the distance which produced μ propagated.

In this way, we obtained the distributions of energy deposit in the detector for neutrinos and charged leptons propagation. These results are used to evaluate the IceCube sensitivity on EHE cosmic neutrinos given by various models.

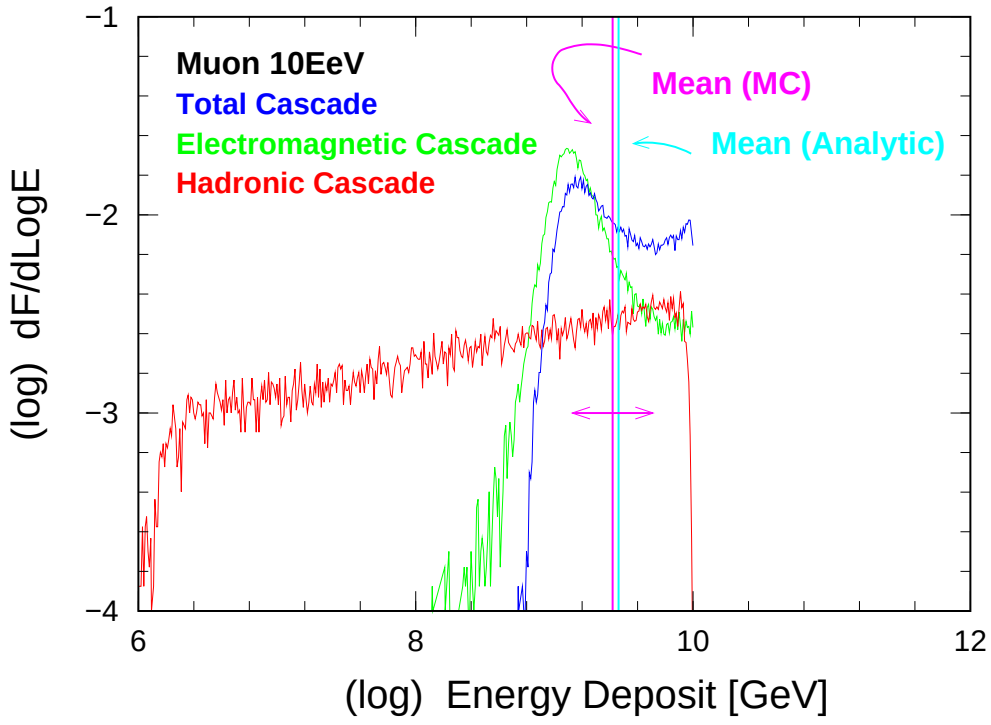

Figure 3.5: Distribution of energy deposit in 1km ice for muon. The green line shows the energy deposit by electromagnetic cascade, the red line for hadronic cascades, and the blue line for the total energy deposit in 1km ice. The unit of $dF/dLogE$ is arbitrary.

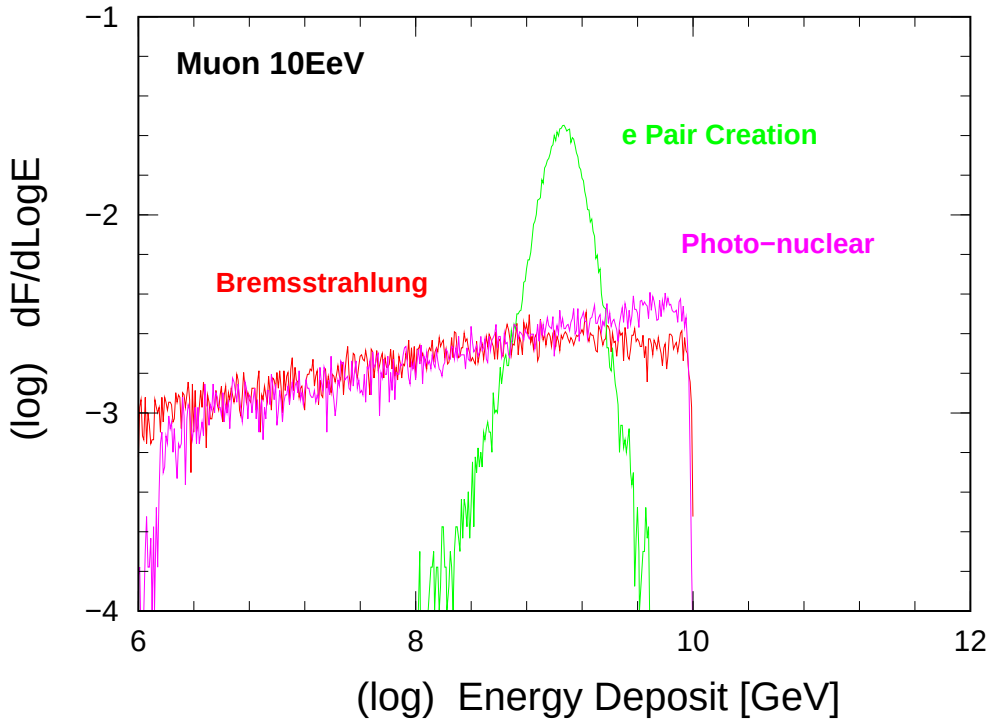

Figure 3.6: Distribution of energy deposit in 1km ice for muon. The contributions from pair creation, bremsstrahlung and photo-nuclear interaction are shown respectively.

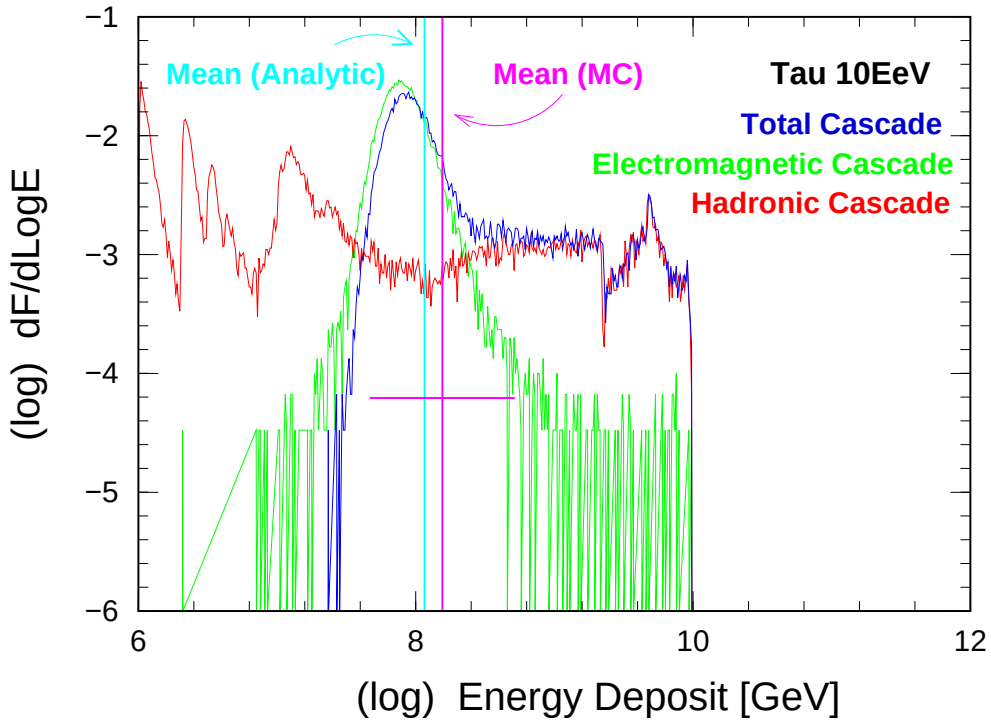

Figure 3.7: Distribution of energy deposit in 1km ice for tau. The green line shows the energy deposit by electromagnetic cascade, the red line shows that by hadronic cascades. The blue line shows the total energy deposit in 1km ice. The unit of $dF/dLogE$ is arbitrary.

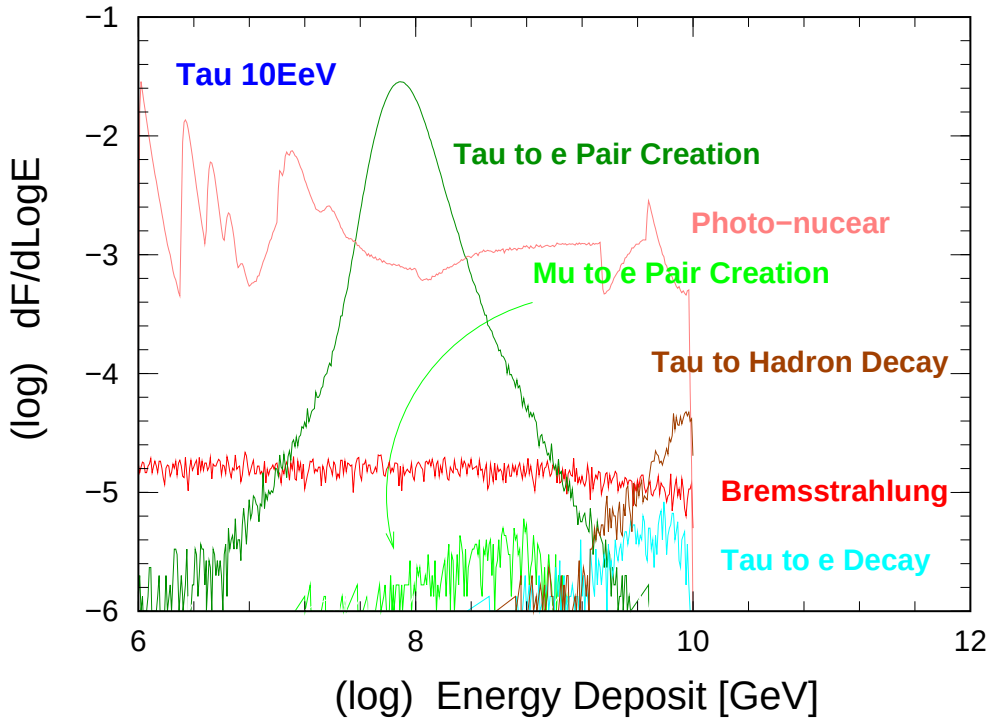

Figure 3.8: Distribution of energy deposit in 1km ice for tau. The line of photo-nuclear interaction is very instable because the cross section of photo-nuclear interaction has large uncertainty.

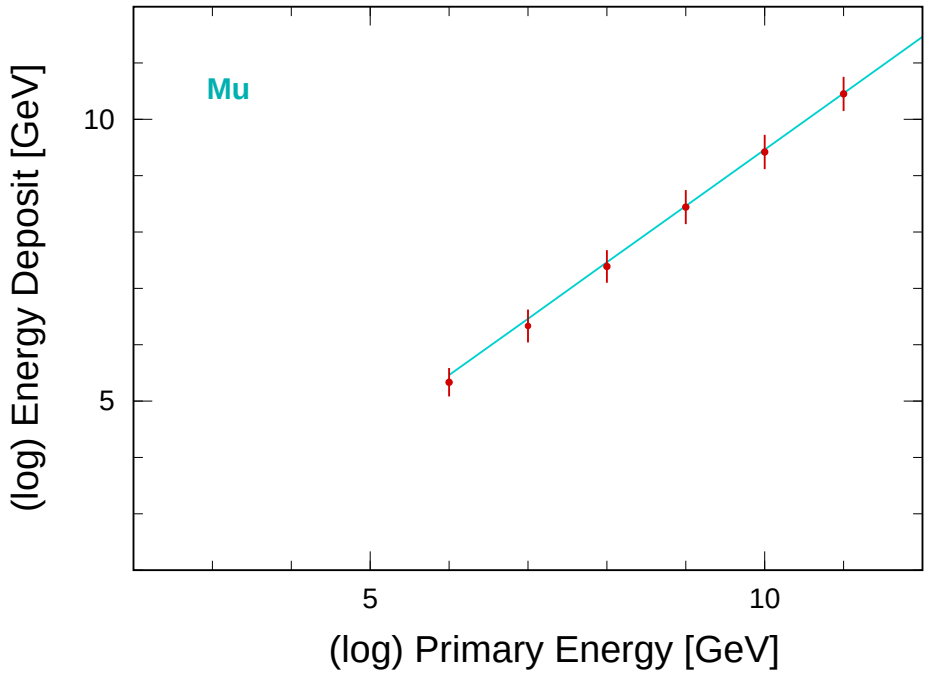

Figure 3.9: Dependence of energy deposit on the primary energy for muon. The red points shows the energy deposit obtained by Monte-Carlo simulation, and blue line shows the analytical value.

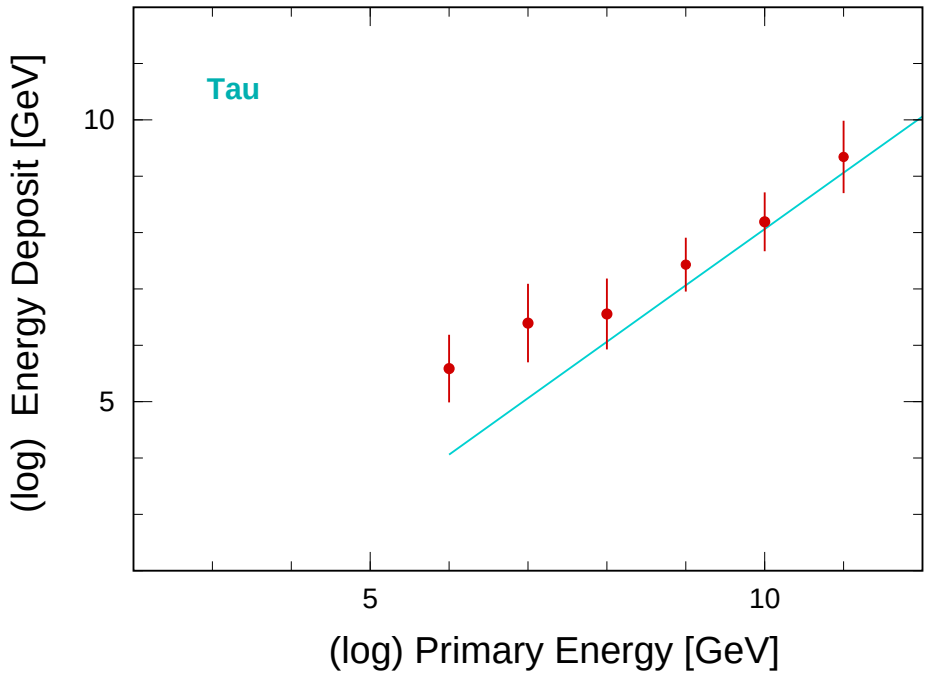

Figure 3.10: Dependence of energy deposit on the primary energy for tau. The red points shows the energy deposit obtained by Monte-Carlo simulation, and blue line shows the analytical value. The departure from the analytical estimation which is visible below 10^8 GeV is due to the contributions by the τ decay.

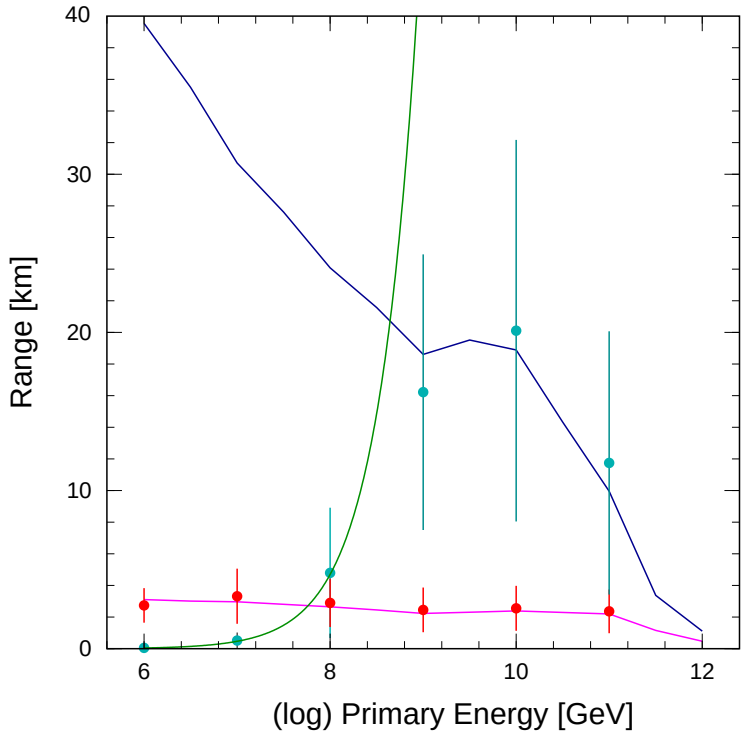

Figure 3.11: Dependence of the range on the primary energy for μ (magenta) and for τ (blue). The point data shows the energy deposit obtained by Monte-Carlo simulation, and line data shows the analytical value.

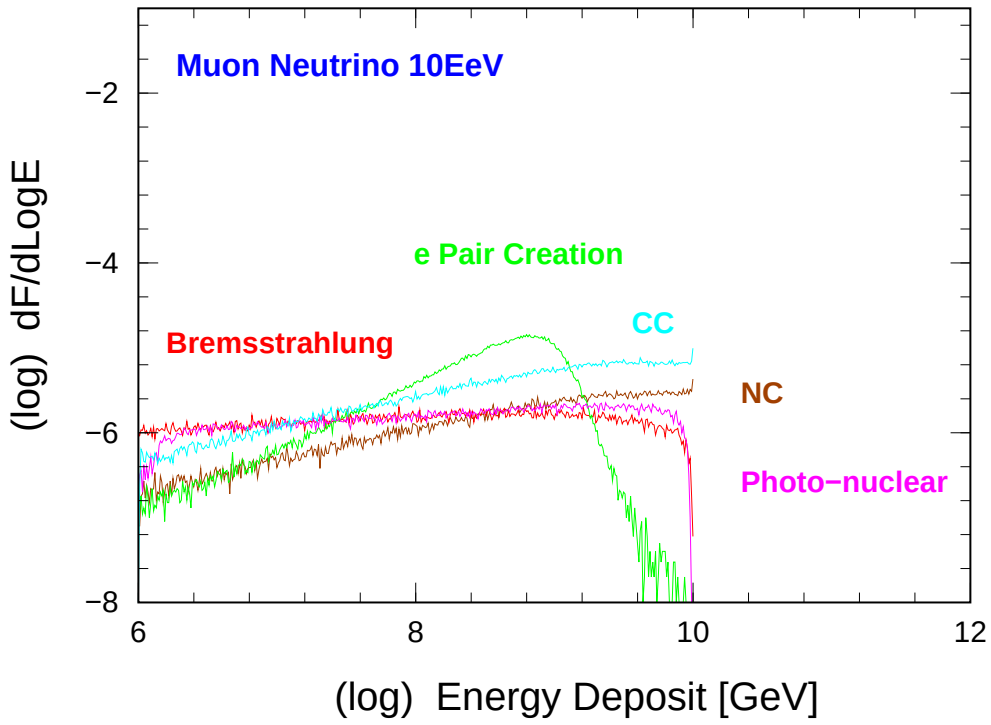

Figure 3.12: Distribution of energy deposit of each interaction in 1km ice for ν_μ. The NC interaction produce hadronic cascades. The CC interaction also produce hadronic cascades, and produced μ induces the interaction such as pair creation, bremsstrahlung and photo-nuclear interaction. The long tail shown in pair creation indicates the difference of the location where the μ was propagated.

Chapter 4

IceCube Sensitivity for EHE Neutrinos

4.1 Flux of Neutrinos and Charged Leptons at IceCube Depth

As described in chapter 3, the JULIeT has a capability to simulate propagation of neutrinos and charged leptons in the earth. Here we calculate the fluxes of neutrinos and charged leptons by propagating the primary EHE neutrinos at the detector depth using the transfer matrices which are generated a priori by PropagationMatrix class in the propagation package (See 3.2.5). Full mixing of ν oscillation is assumed and made proper adjustment in the primary flux of EHE cosmic neutrinos.

Table 4.1 summarized the EHE neutrino models and their parameters, which we used for estimation of the EHE cosmic neutrino flux at the surface.

They are input spectra to our propagation calculation, then we discuss the IceCube sensitivity for EHE neutrino fluxes taking into account their propagation effects in the earth and the energy deposit characteristics of the secondary leptons.

4.1.1 GZK Neutrinos

The models **1∼6** [16] and **10, 11** [20] in Table 4.1 are the GZK neutrino models. The GZK neutrinos are generated via decays of charged pions which are produced by photo-pion production of EHECRs colliding CMB photons. This production chain,

$$\begin{aligned} p\gamma &\rightarrow \pi^{\pm} + anything \\ &\rightarrow \mu^{\pm} + \nu_{\mu}(\bar{\nu}_{\mu}) \\ &\rightarrow e^{\pm} + \nu_{e}(\bar{\nu}_{e}) + \bar{\nu}_{\mu}(\nu_{\mu}), \end{aligned}$$

does not have any channel to produce ν_{τ}. There is no ν_{τ}s are primarily produced within the GZK neutrino production.

The GZK model **1∼6** from Ref. [16, 17] has a few parameters concerning the cosmic ray source distribution. m is the evolution parameter which relevant to the luminosity of EHECR as a function of red shift ($m = 0$ corresponds to the no evolution). Z_{max} is the "turn-on time", which means the time when EHECR were created. γ indicates the energy spectrum of primary EHECRs following $E^{-\gamma}$.

	model	m	Z_{max}	γ	$Emax[ZeV]$
1	The GZK Neutrinos	0	2		
2	The GZK Neutrinos	2	2		
3	The GZK Neutrinos	2	4		
4	The GZK Neutrinos	4	4		
5	The GZK Neutrinos	4	5	1.5	
6	The GZK Neutrinos	7	5	1.5	
7	The Z-burst				
8	The Top Down (SUSY)				
9	The Top Down (QCD)				
10	The GZK Neutrinos (by Sigl)	3	2	1	100
11	The GZK Neutrinos (by Sigl)	5	2	2	10

Table 4.1: EHE neutrino models. Model-1∼6 are GZK Neutrinos [16], Model-7 is Z-burst model [18], Model-8,9 are Top Down models [19], Model-10,11 are GZK Neutrinos [20]. The m, Z_{max}, γ, and $Emax[ZeV]$ are parameters which individualize the models. Note that there is no ν_τ in GZK model.

The another GZK model **10** and **11** from Ref. [20] has one more parameter, E_{max} is the maximum energy of primary EHECRs.

4.1.2 Z-burst

The Z-burst model [18] is about interactions of EHECRs with cosmic background neutrinos which are a relic of the Big Bang. The cross section of the interaction has a resonance when the collision energy is the mass of Z_0 boson. The produced charged leptons or hadrons induce the neutrino cascade. This cascade can produce the EHE particles above GZK threshold.

4.1.3 Top Down Scenario

The model **8, 9** in the Table. 4.1 is the top down scenario [19]. This scenario supposes that the EHE cosmic rays and neutrinos are produced from massive particles via an interaction/decay. The top down scenario may be able to explain the existence of EHE cosmic rays beyond GZK cut-off.

4.2 Background

The backgrounds in detecting EHE cosmic neutrinos are atmospheric muons and neutrinos. They are produced via the decay of mesons produced by the interaction of cosmic rays with atmosphere. The atmospheric muons and neutrinos can arrive at the detector depth.

Since the energy spectrum of atmospheric neutrinos falls steeply like $dN_\nu/dE_\nu \sim E^{-3.7}$, the EHE cosmic neutrino energies extend to higher values. The dependence of the flux on the zenith angle can be characterized by

$$\frac{dF}{dE} = kE^{-(\gamma+1)} \left(\frac{1}{\frac{1}{1+1.1(E/E_1)\cos\theta} + \frac{0.054}{1+1.1(E/E_2)\cos\theta}} \right), \tag{4.1}$$

where the cosmic ray flux is proportional to $E^{-\gamma}$, E_1 =115GeV and E_2 =850GeV are the factors due to the dependence of path length on the zenith angle. The atmospheric muons should contribute to only the down-going events. The energy spectrum of atmospheric muons may be steeply enough to be distinguished from signal events by setting a propaer threshold energy in filtering.

4.3 Flux at the IceCube Depth

Figure 4.1 shows the angular distributions of the relevant fluxes above 10 PeV of μ and τ at the detector after propagation in the earth. The fluxes of μ and τ are calculated by propagating the primary GZK neutrinos (with $m = 4$, $Z_{max} = 4$ in Ref. [16]) in the earth. It should be noted that the full mixing of ν oscillation of the primary cosmic neutrino is assumed *i.e.,* $\nu_e : \nu_\mu : \nu_\tau = 1 : 1 : 1$. The intensity of the fluxes strongly depends on zenith angle. The up-going particles are strongly attenuated by the earth, because they have to propagate a distance longer than down-going particles The main contribution to the fluxes is the down-going events ($\cos\theta \geq 0$, θ is the zenith angle of incident particle). The flux of τ is larger than that of μ in up-going and horizontal region. It indicates that the detecting τ events with up-going and horizontal angle is advantageous. The reason the τ has larger flux is that the τ propagate in th earth with losing its energy slowly compared with μ regeneration process like $\nu_\tau \to \tau \to \nu_\tau$ also contributes the flux.

There are two lines of the fluxes of atmospheric muons are also shown in Figure 4.1. The one is calculated by the extrapolation from the flux of 5 TeV with assuming that cosmic ray spectrum has $E^{-2.7}$ form and the another is given by Corsika [22] with assuming E^{-3}. The contribution of atmospheric muons is, however, also large where $\cos\theta \geq 0$. Figure 4.2 shows the angular distributions of fluxes which *deposit* their energy above 10 PeV. The contribution of atmospheric muon is small because the energy of them is relatively lower than that of μ and τ.

It also shows that the horizontal events ($\cos\theta \sim 0$) are the mostly responsible for an observed bulk of EHE events.

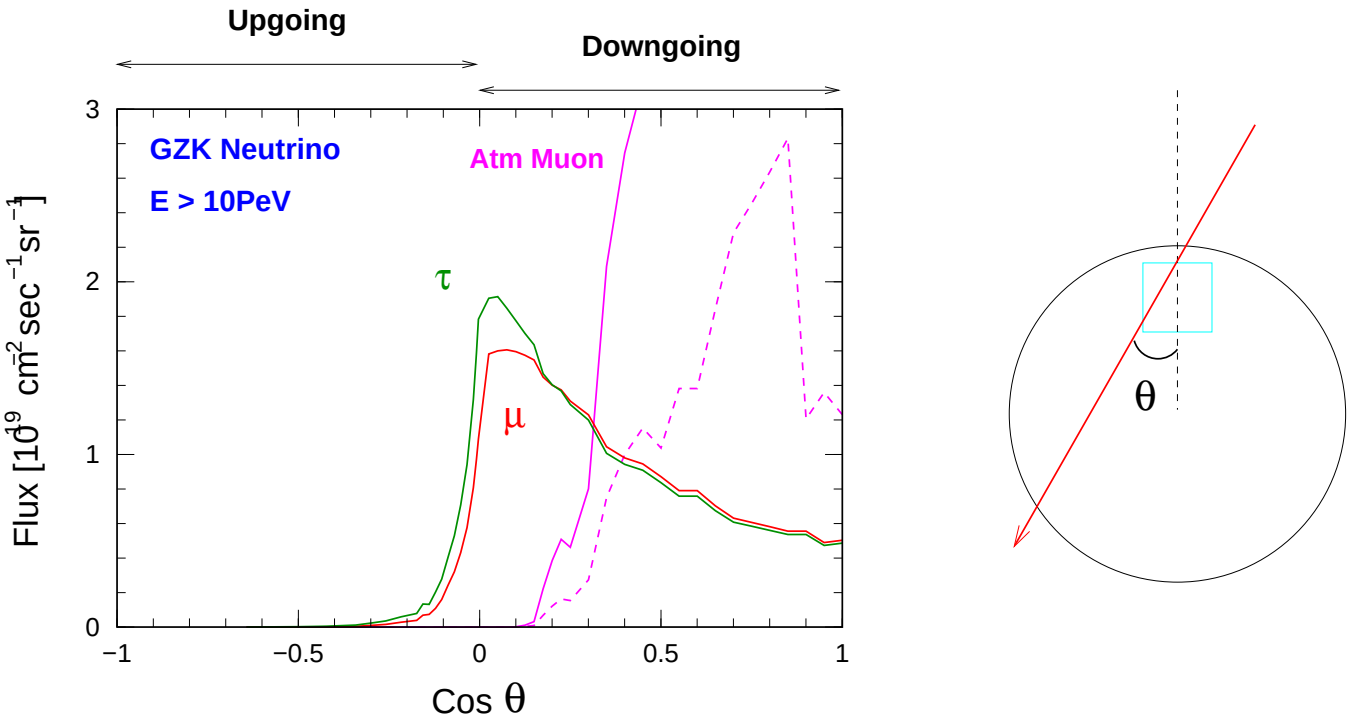

Figure 4.1: The angular distributions of fluxes of μ and τ after propagation in the earth. The fluxes above 10 PeV are plotted. θ is zenith angle of incident neutrinos defined as the right-side figure. In the case of $\cos\theta \geq 0$, it indicates down-going events. The primary neutrinos are given by GZK model in Ref. [16] with $m = 4$, $Z_{max} = 4$. The fluxes of atmospheric μ are also plotted, solid line is given by the extrapolation from 5 TeV, dashed line is given by Corsika estimation [22].

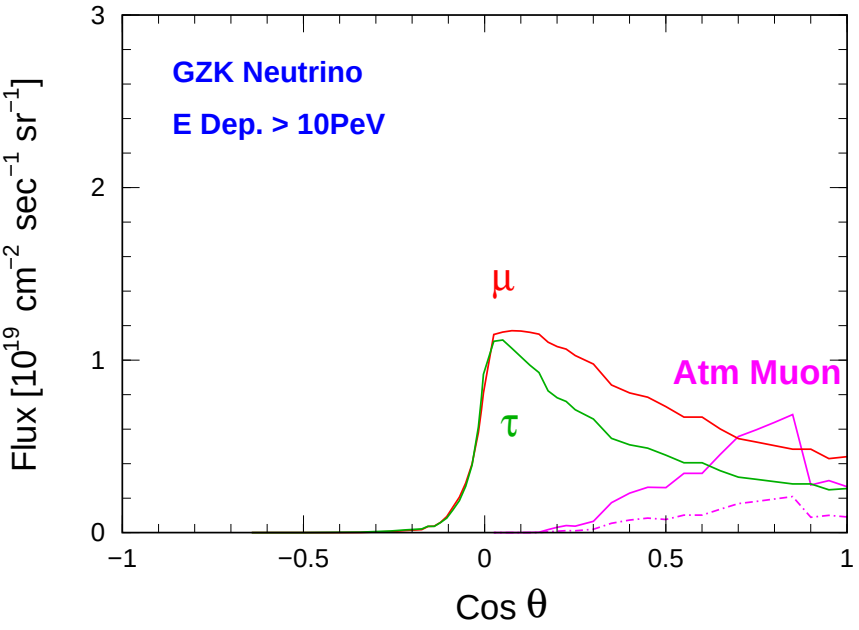

Figure 4.2: The angular distributions of energy deposit in the detector for μ and τ. The fluxes which deposit their energy above 10 PeV are plotted. θ is zenith angle of incident neutrinos. The primary neutrinos are given by GZK model in Ref. [16] with $m = 4$, $Z_{max} = 4$. The fluxes of atmospheric μ are also plotted, solid line is given by the extrapolation from 5 TeV, dashed line is given by Corsika estimation [22].

4.4 Evaluation of IceCube Sensitivity

The IceCube sensitivity is evaluated by the event rate per energy decade $dN/dLogE$. In order to obtain the fluxes of neutrinos and charged leptons incident to the detector as a function of zenith angle, the numerical transportation in the earth is carried out for a given flux of primary neutrinos. Then convoluting the results of Monte-Carlo simulation, we obtained the IceCube sensitivity.

Figure 4.3 shows the resultant sensitivity with $1km^2$ detection area for ν_μ and for ν_τ, respectively. The various model predictions are also plotted together for comparison. The event flux which lose the energy above threshold is calculated by Monte-Carlo simulation described in section 3.3. The obtained energy rate is integrated over zenith angle. The 90% C.L. upper limit, *i.e.,* (2.3 events)/(10 years)/($1km^2$ detection area)/(energy decade), for the threshold of the energy deposit in the detector for 1 PeV and 10 PeV are shown.

The ν_τ sensitivity is better than that of ν_μ above 10^9 GeV region because the detection volume of τ is larger than that of μ. While, below 10^9 GeV region, the ν_μ sensitivity is better than ν_τ sensitivity, because the energy deposit of μ is basically larger than the case of τ (See Figure 3.10 and 3.9). But, the ν_μ sensitivity has a bump structure around 10^8 GeV region. It is due to the contribution of the τ decay which induces large energy deposit.

Additionally, Figure 4.4 shows the sensitivity which include *both* ν_τ and ν_μ contributions. This figure indicates that the model above the lines of threshold can be excluded in absence of signals with 90% C.L.. The solid blue lines show the limits obtained by the case of the incident particle is charged leptons. While the dashed lines show the limits in the case of the charged leptons produced via CC inside the detector. Below 10^8 GeV region, charged leptons must be produced near the detector volume to remain their energies above the threshold, which leads to reduction of the detector volume, while energy deposit at the CC/NC vertex contributes total energy loss in significant way in case of neutrino primary events. The resultant sensitivity around the threshold energy will be, consequently, enhanced by looking at not just muon/tau tracks but neutrinos inducing cascades inside the detector volume. From Figure 4.4, the IceCube has the sensitivity enough to exclude the GZK model which is the most solid model for the EHE cosmic neutrinos.

The Table 4.2 shows 90% C.L. upper limit of primary EHE neutrino fluxes, which are placed by E^2dF/dE [GeV cm^{-2} sec^{-1} sr^{-1}] form.

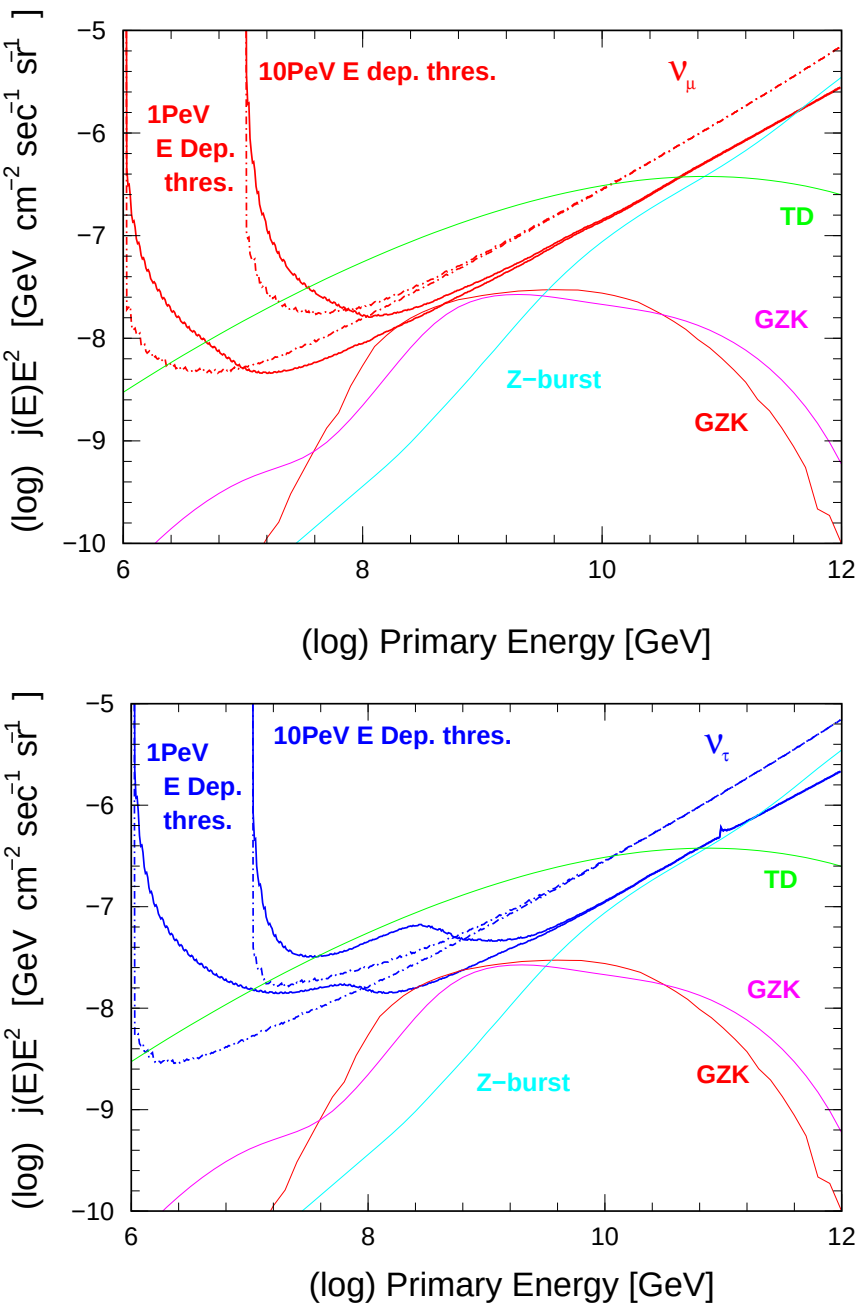

Figure 4.3: The IceCube sensitivities on the EHE neutrino fluxes. The upper figure shows the ν_μ sensitivity, and the lower figure shows the ν_τ sensitivity. The 90% C.L. upper limits of the primary neutrino flux by a $1km^2$ detection area with 10 years operation for the threshold energies with 1 PeV and 10 PeV are plotted. The solid blue lines show the limits obtained in the case of the incident particle is charged leptons. While the dashed lines show the limits by the case of the charged leptons are produced via CC inside the detector. The other lines indicate the various model predictions given by, GZK ([16] with (m, Z_{max})=(4, 4) for the red line, [20] with $(m, Z_{max}, \gamma, E_{max})$=(5, 2, 2, 10 ZeV) for the magenta line), TD [19] and Z-burst [18].

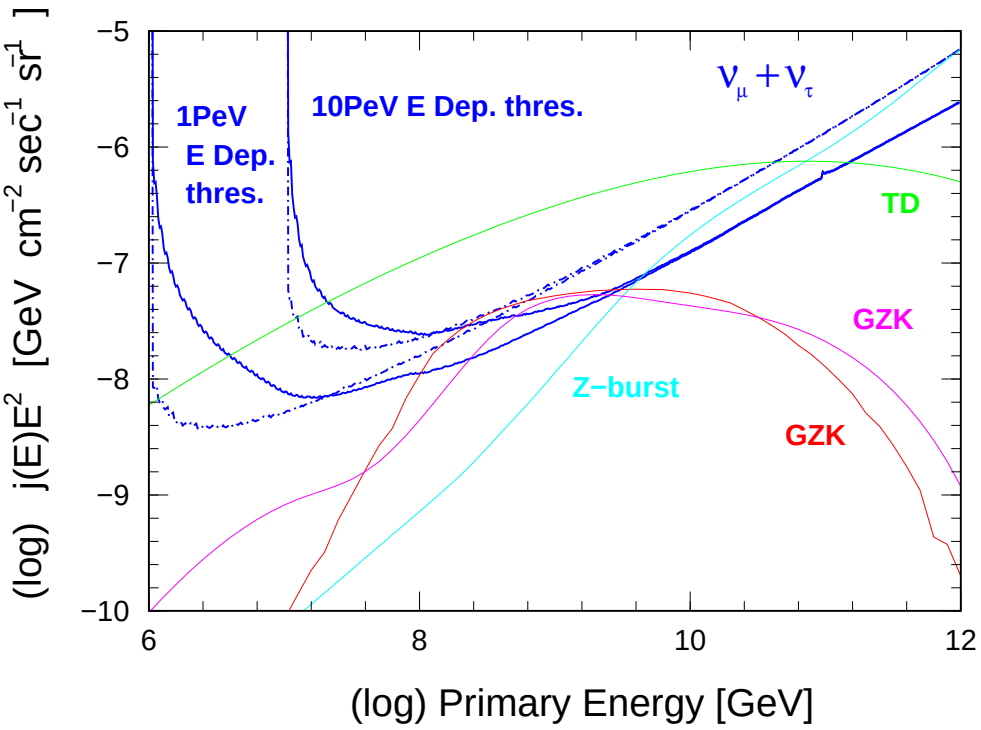

Figure 4.4: The IceCube sensitivities on the EHE neutrino fluxes. The blue lines show the sensitivities which include *both* ν_τ and ν_μ contributions. The solid thick lines show the limits obtained by the case of the incident particle is charged leptons. While the dashed lines show the limits by the case of the charged leptons are produced via CC inside the detector. Same as Figure 4.3, the various models predictions are also plotted.

	ν_μ	ν_τ	$\nu_\mu + \nu_\tau$	$\nu_\mu + \nu_\tau$/flavor
1 PeV thres.	3.3×10^{-8}	3.0×10^{-8}	3.2×10^{-8}	1.6×10^{-8}
10 PeV thres.	3.7×10^{-8}	4.6×10^{-8}	4.1×10^{-8}	2.1×10^{-8}

Table 4.2: 90% C.L. upper limit for EHE neutrino fluxes, which are given by $E^2 dF/dE$ [GeV cm^{-2} sec^{-1} sr^{-1}] form are shown with the primary EHE neutrinos' energies of 10^9 GeV. Rows are threshold energy deposit and columns are primary neutrinos. The threshold energy with 1 PeV and 10 PeV are shown.

Chapter 5

Summary and Outlook

5.1 Summary

We developed the MonteCarlo/Numerical simulator "JULIeT" for transporting the neutrinos and charged leptons for the IceCube.

The JULIeT was developed in order to understand *both* the EHE particles propagation in the earth and in the detector. As fundamental checks of JULIeT, we calculated the distributions of energy deposit in $1km$ ice for μ and τ. They shows the fluctuation which are affected by stochastic interactions such as bremsstrahlung, photo-nuclear and so on. In the case of τ, especially, the contribution of decay is not negligible in lower energy range. The dependence of energy deposit on the primary particle's energy also shows that the contribution of τ decay is sizable.

The JULIeT still has a problem, arisen from the uncertainty of the cross section of the photo-nuclear interaction. The instability of this cross section adversely affect on all the results we obtained.

We calculated the propagation in the earth by numerically solving transport equations. We obtained the incident fluxes of these particle to the detector by transporting the primary EHE neutrinos given by various models. While, by using the Monte-Carlo methods, we calculated the energy deposit distribution of the particles in the detector made of ice.

By combining those results, we obtained the energy deposit distribution of the neutrinos and charged leptons produced by EHE cosmic neutrinos. The event rate for given EHE neutrino fluxes was obtained to evaluate the IceCube sensitivity. The 90% C.L. upper limits for the primary EHE neutrino fluxes, *i.e.,* (2.3 events)/(10 years)/($1km^2$ detectionarea)/(energy decade), for the threshold energies with 1 PeV and 10 PeV were estimated as a function of primary neutrino energy. The resultant upper limits for 10 PeV threshold would be placed at $E^2dF/dE \simeq 3.7 \times 10^{-8}$ [GeV cm^{-2} sec $^{-1}$ sr $^{-1}$] for ν_μ, and 4.6×10^{-8} [GeV cm^{-2} sec $^{-1}$ sr $^{-1}$] for ν_τ with 10^9 GeV. We also calculated the 90% C.L. upper limits for the sum of ν_μ and ν_τ origin events; 2.1×10^{-8} [GeV cm^{-2} sec $^{-1}$ sr $^{-1}$ flavor^{-1}] with 10^9 GeV threshold.

5.2 Future Work

The highest-priority issue for the progress of the JULIeT is the improvement of the parameterization of differential cross sections of photo-nuclear interaction. The instability of the photo-nuclear cross section adversely affect on all the results we obtained.

The JULIeT in the current version is not able to simulate cascade development. Instead, it sim-

ply records primary energy of the electron(or photon)/hadron (i.e. primary energy of the electromagnetic/hadronic cascades) and its generated location, *i.e.* it sees the cascades as point like. In order to understand the Cherenkov light from cascades with accuracy, the JULIeT should be able to simulate the cascade development with Monte-Carlo methods.

The detector defined in the current version of the JULIeT is just an ice, in which the DOMs have not instrumented yet. It needs a class to define the geometry of DOMs in the points package of the JULIeT.

Bibliography

[1] K. Greisen, Phys. Rev. Lett. **16**, 748, 1966.

[2] IceCube Collaboration, astro-ph/0305196, (2003).

[3] R. Gandhi, C. Quigg, M. H. Reno and I. Sarcevic, Phys. Rev. D **58**, 093009, 1998.

[4] H. L. Lai *et al.*, Phys. Rev. D **55**, 1280, 1997.

[5] P. Miočinović, Ph.D. thesis, (2001).

[6] R. P. Kokoulin and A. A. Petrukhin, Proc. of the 12th ICRC, Vol.6 p.A2436, (1971).

[7] S. R. Kelner, R. P. Kokoulin and A. A. Petrukhin, Phys. At. Nucl. **62**, 1894, (1999).

[8] Yu. M. Andreev, L. B. Bezrukov and E. V. Bugaev, Phys. At. Nucl. **57**, 2006, (1994).

[9] S. R. Kelner, R. P. Kokoulin and A. A. Petrukhin, Phys. At. Nucl. **60**, 576, (1997).

[10] I. A. Sokalski, E. V. Bugaev and S. I. Klimushin, Phys. Rev. D **64**, 074015, (2001).

[11] S. Yoshida, *Ultra-High Energy Particle Astrophysics*, (Nova Science Publishers, Inc., New York, U.S., 2003).

[12] S. I. Dutta, M. H. Reno, I. Sarcevic, Phys. Rev. D **62**, 123001, (2000).

[13] S. I. Dutta, M. H. Reno, I. Sarcevic and D. Seckel, Phys. Rev. D **63**, 094020, (2001).

[14] H. Abramowicz and A. Levy, hep-ph/9712415, (1997).

[15] S. Yoshida, R. Ishibashi and H. Miyamoto, astro-ph/0312078, accepted for publication in Phys. Rev. D **69**, (2004).

[16] S.Yoshida *et al.*, The Astrophysical Journal, **479**, 547-559, (1997).

[17] S. Yoshida and M. Teshima, Prog. Theor. Phys., **89**, 833, (1992).

[18] S.Yoshida, G. Sigl and S. Lee, Phys. Rev. Lett., **81**, 5505, (1998).

[19] G.Sigl *et al.*, Phys. Rev. Lett., D **59**, 043504, (1998).

[20] O. E. Kalahsev, G. Sigl *et al.*, Phys. Rev. Lett., D **66**, 063004, (2002).

[21] V. Agrawal *et al.*, Phys. Rev. Rev., D **55**, 1314, (1996).

[22] D. Heck *et al.*, Report FZKA **6019**, (1998).